UiT
THE ARCTIC
UNIVERSITY
OF NORWAY

FACULTY OF SCIENCE AND TECHNOLOGY
DEPARTMENT OF GEOLOGY

Multibeam bathymetry and backscatter data analysis of pockmarks at Vestnesa Ridge off NW-Svalbard

Glennda Alina Villaflor

Master's Thesis in Geology
November 2014

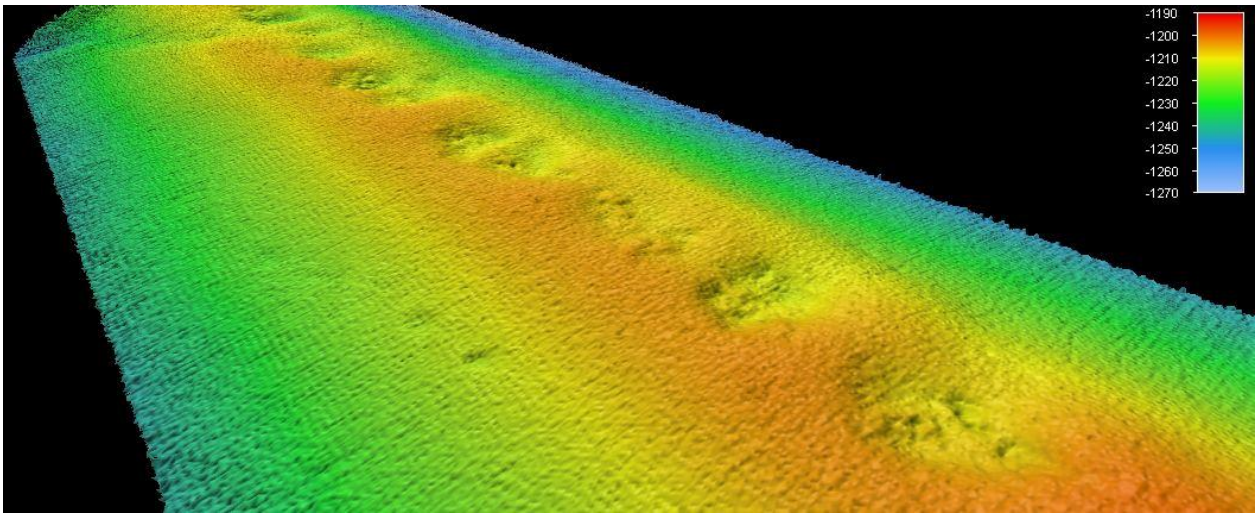

UNIVERSITY OF TROMSØ

Geo 3900

Master's Thesis in Geology

Multibeam bathymetry and backscatter data analysis of pockmarks at Vestnesa Ridge off NW-Svalbard

Glennda Alina Villaflor

November 2014

ABSTRACT

The Vestnesa Ridge is an elongated sediment drift situated at 79° N on the northwest Svalbard margin in the Fram Strait. It is one of the northernmost documented oceanic gas hydrate provinces. The narrow southeastern part of the ridge is characterized by pockmarks that line up along the apex of the crest. Some of these pockmarks are continuously venting gas while some are inactive. This study looks at changes in morphology of the pockmarks in relation to sedimentary processes, ocean currents and fluid flow mechanism, and their role in active fluid venting. Detailed bathymetry and backscatter data from different surveys in 2010, 2012 and 2013 are studied. Comparing the surfaces reveals relatively less sediment deposition in the pockmarks. The pockmarks exhibit an elongate shape and asymmetrical profiles, pointing to a strong influence by the WSC bottom currents. Backscatter data also reveal possible carbonate or gas hydrate deposits inside the pockmarks. These observations, along with apparent inactivity in some pockmarks, point to a possible scenario where carbonate or hydrate formation leads to self-sealing and eventual relocation of the gas vents through existing faults and fractures.

ACKNOWLEDGEMENTS

I would like to thank my adviser Dr. Stefan Bünz and the Geology Department for letting me write this thesis. I am forever grateful for the opportunity.

I would also like to thank my family for the support and love.

Maraming salamat.

Glennda Villaflor

Tromsø, November 2014

Table of Contents

1 INTRODUCTION

1.1 PURPOSE

The aim of this master thesis is to map and describe morphological changes on the seabed of the Vestnesa Ridge along the continental margin west of Svalbard. Swath bathymetry gridded to 10 m from three different cruises from 2010, 2012 and 2013 were processed using QPS Fledermaus 4D geo-spatial processing and analysis tool for high resolution imaging of the seabed. The results will show in changes in the local geomorphology that may be related to sedimentary processes, ocean currents and fluid flow activity in the area. In addition, backscatter data will also be analyzed using QPS Fledermaus Geocoder Toolbox (FMGT) to identify structures or deposits related to fluid flow and to classify the different types of sedimentary environment in the study area.

1.2 STUDY AREA

The study area is located at the Vestnesa Ridge situated on the northwest Svalbard margin in the Fram Strait. The Vestnesa Ridge is a SE-NW to E-W bending elongated sediment drift situated at 79° N to the northeast of the Molloy transform fault and to the north of the Knipovich Ridge (Figure 1). It is one of the northernmost documented oceanic gas hydrate provinces, with active gas leakage at the eastern part on the upper continental slope (Bünz et al., 2012).

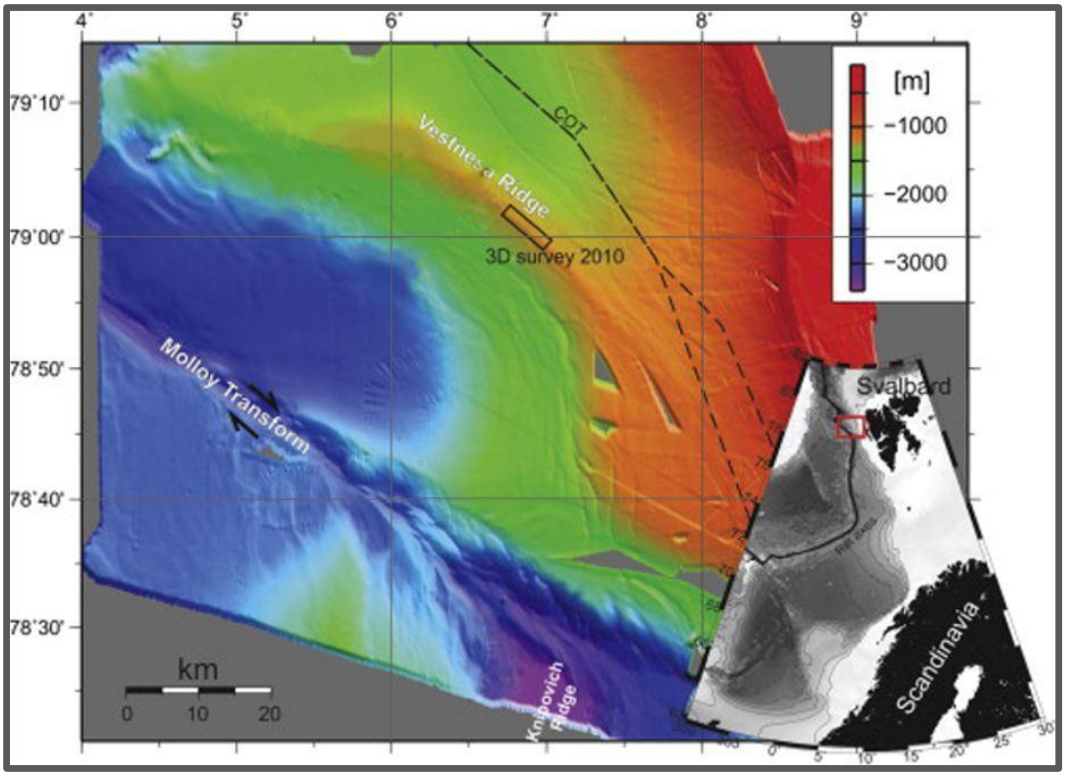

Figure 1: Overview map of the Vestnesa Ridge on the western margin of Svalbard. (modified from Bünz et al., 2012)

1.3 FLUID FLOW

Seabed fluid flow involving seepage of free methane gas and/or water with a high methane concentration in solution is found in every sea and ocean (Judd, 2003). Acoustic and seismic data can reveal seabed fluid flow indicators such as pockmarks, mud volcanoes, acoustic chimneys, pingos and authigenic carbonate build up which are related to hydrocarbon migration (Hovland and Judd, 1988). These may be present both in passive continental margins in areas with rapid sedimentation and undercompaction that prevents fluids to be expelled during sedimentation, and on active continental margins, where they are mainly related to compressional geological processes (Judd and Hovland, 2007).

Pockmarks are craters that commonly occur worldwide on muddy seabed and are known to occur on continental slopes with gas hydrates and in association with slides and slumps (Hovland et al., 2002). They occur wherever fluid flow is focused and escape is from low-permeability, fine-grained surficial sediments (Hovland and Judd, 1988). Pockmarks can be subdivided into six morphological classes (Hovland et al.2002) (Figure 2):

- *Unit pockmarks* are small depressions typically 1-10 m across and up to 0.5 m deep, and probably represent a one-time expulsion event. They are common inside and around normal pockmarks.

- *Normal pockmarks* are circular depressions typically 10-700 m across, and from 1-45 m deep. Their cross-section varies from a basin-formed (low-angle) shape to an asymmetrical and steep-walled feature. Some are even funnel-shaped in the center.

- *Elongated pockmarks* are depressions with one axis that is much longer than the other. They occur on slopes and areas of seafloor influenced by strong bottom currents.

- *Eyed pockmarks* contain an acoustically high-reflective object or region in its central part, which could either be caused by coarse material remaining after the erosive process (winnowing), from biological activity (skeleton remains, dead and living shells, etc.) or from authigenic carbonate precipitation.

- *Strings of pockmarks* consist of unit pockmarks or small normal pockmarks arranged in curvilinear chains or strings, which may be kilometers in length. They are suspected to be a result of fluid focusing along near-vertical faults, flexures or weakness zones in the upper sedimentary layer.

- *Complex pockmarks* occur as clusters of normal pockmarks or amalgamations of large pockmarks.

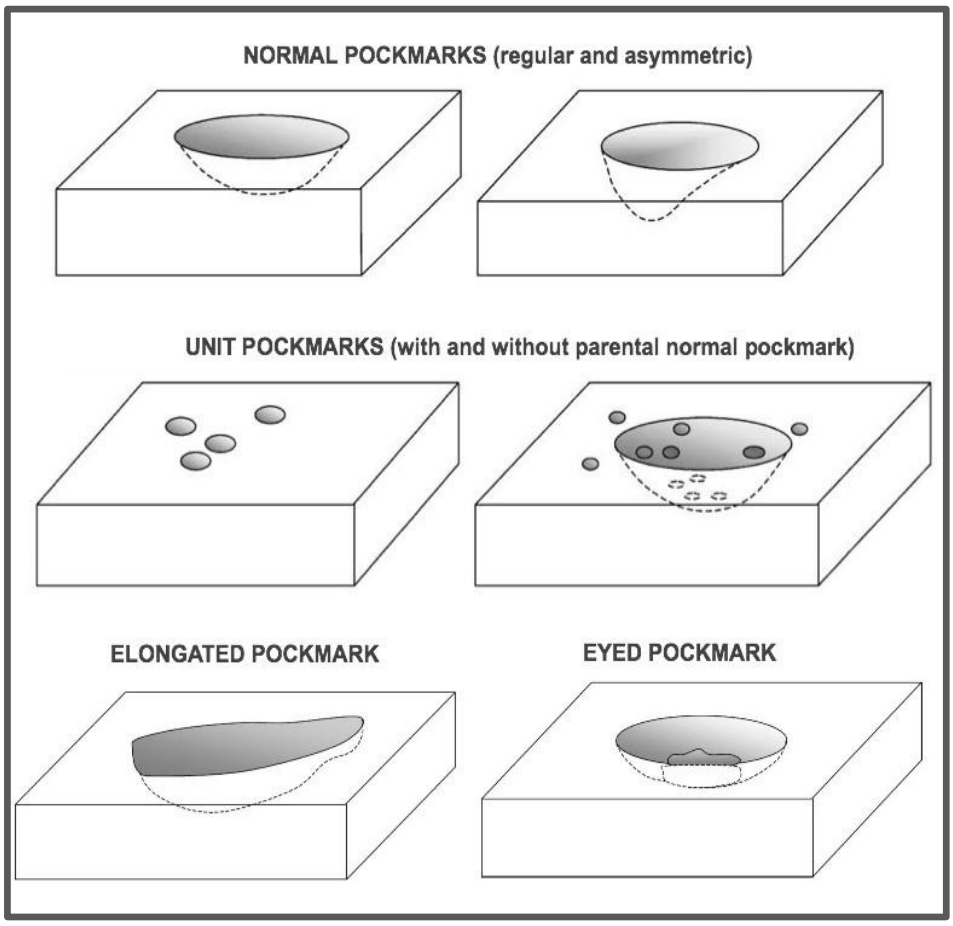

Figure 2: Illustration of the main morphological classes of pockmarks. (adapted from Hovland et al., 2002)

Fluid migration may be detected on seismic data where acoustic masking and its related features occur. Acoustic masking is an area on the seismic profile with low seismic reflectivity or where the reflections are highly distorted or disturbed. When occurring in association with other gas indicators such as bright spots or pull down of underlying seismic reflections, they may be interpreted to indicate a scattering of acoustic energy caused by interstitial gas bubbles in sediments (Anderson and Hampton, 1980) (Figure 3). Gas chimneys are detected on seismic data as vertical zones which have been disturbed by previous or ongoing gas migration. The acoustic disturbance in the chimneys may have been caused by small parcels of gas in the pore space of sediments and slightly displaced sediments (Judd and Hovland, 2007). Rapid and strong gas flows may cause upward directed structural disturbances of sediment layers and a blow-out feature at the sediment surface. Acoustic gas chimneys may show both push down and pull-up effects. Pull up may occur in the presence of a high velocity zone in layers of authigenic carbonate or gas hydrates.

Pockmarks on continental shelves and slopes, in estuaries and in lakes may be considered as valuable monitoring sites for deep fluids (Hovland et al., 2002).

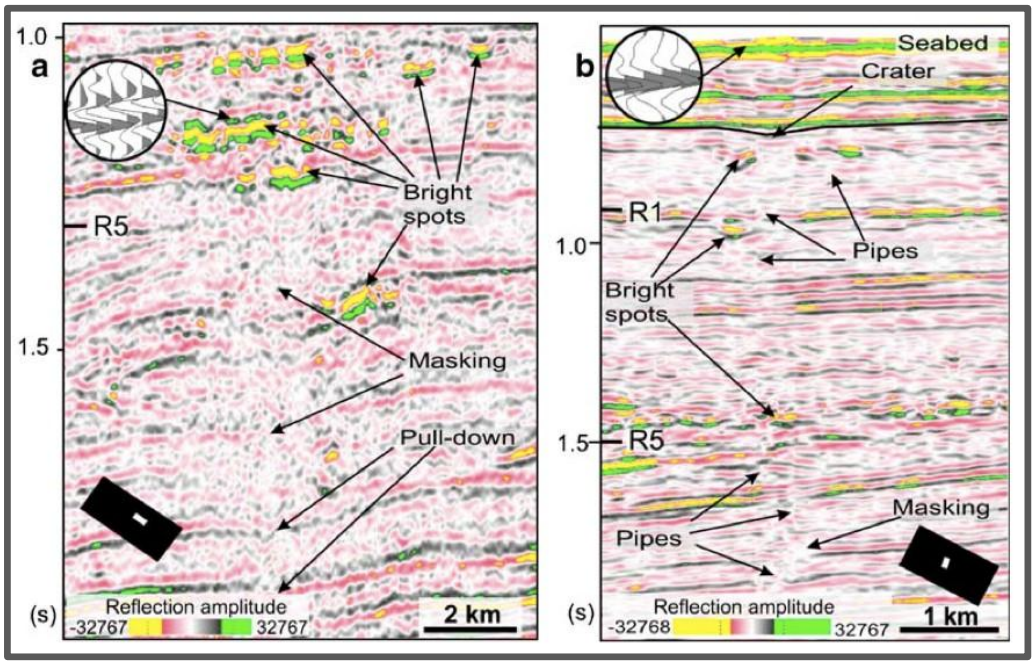

Figure 3: (a) Seismic profile showing a zone of acoustic masking, associated bright spots and pull down of underlying reflections. (b) Seismic profile showing acoustic pipes interpreted to represent fractures pathways for gas-bearing fluids, leading in this case to an interpreted pockmark crater on the buried horizon. (from Andreassen et al., 2007)

1.4 GAS HYDRATES

Gas hydrates are crystalline solids and are similar to ice, except that the crystalline structure is stabilized by a gas molecule within the cage of water molecules (Judd and Hovland, 2007). Many gases have molecular sizes suitable to form hydrates, including naturally occurring gases such as methane and other hydrocarbons, although most marine gas hydrates that have been recovered and analyzed are methane hydrates. Natural gas hydrates can be found mainly in oceanic and permafrost regions, where the pressure and temperature conditions are such that gas hydrates remain stable. In addition, there must be an adequate supply of gas molecules and water within the sediments (Hovland, 2005, Kvenvolden, 1993).

Gas hydrates may be indirectly detected using seismic methods, where the base of the gas hydrate stability zone (GHSZ) is indicated by a BSR (bottom simulating reflector) (Figure 4). The base of gas hydrate-bearing sediments follows iso-temperature lines and causes a seismic reflection that is parallel to the seafloor. The BSR may be caused by the high velocity of the gas hydrate in the hydrate-bearing zone above the BSR, or by the low velocity of free gas in the gas-bearing zone below the BSR. In any case, the BSR is characterized by being a negative-polarity reflection, indicating a negative reflection coefficient. The compressional wave velocity decreases abruptly when the seismic signal enters from the hydrated sediments above to gas charged sediments beneath it. Due to the velocity drop, the gas hydrate/free gas related BSR shows a phase reversal if compared to the sea floor. The true nature of BSR is mostly due to the presence of free gas beneath the hydrate sediments (Andreassen et al., 1995). Since the BSR is dependent on pressure and temperature, it may also cross-cut the sedimentary bedding (Bünz and Mienert, 2004).

Natural submarine gas hydrates are regarded as important because it has a potential of being an energy resource – the density of methane hydrates is up to five times greater than the energy density of conventional natural gas (Kvenvolden, 2000). Gas hydrates may also have a strong influence on the environment and climate because methane is a significant greenhouse gas. They may also be a significant geohazard because they alter

the seafloor sediment stability – the permeability of the sediment decreases due to gas hydrate growth and sediment compaction stops. When continued sedimentation causes a deeper burial of gas hydrate, it will then reach a temperature where the gas hydrate is no longer stable. The solid gas hydrate will become a liquid gas/water mixture, and the basal zone of the gas hydrate becomes underconsolidated and possibly overpressured due to newly released gas, leading to a zone of weakness. This zone of reduced shear strength and increased overpressure may result in submarine slope failures (McIver, 1982). A study of the Storegga slide by Mienert et al. (2004) suggests that the hydrate stability zone in the upper part of the Storegga area was significantly influenced by variations in ocean temperature since LGM, and that hydrate dissociation may also have influenced the position of the headwall of the slide, corresponding with the zone of predicted maximal in situ pore pressure build-up.

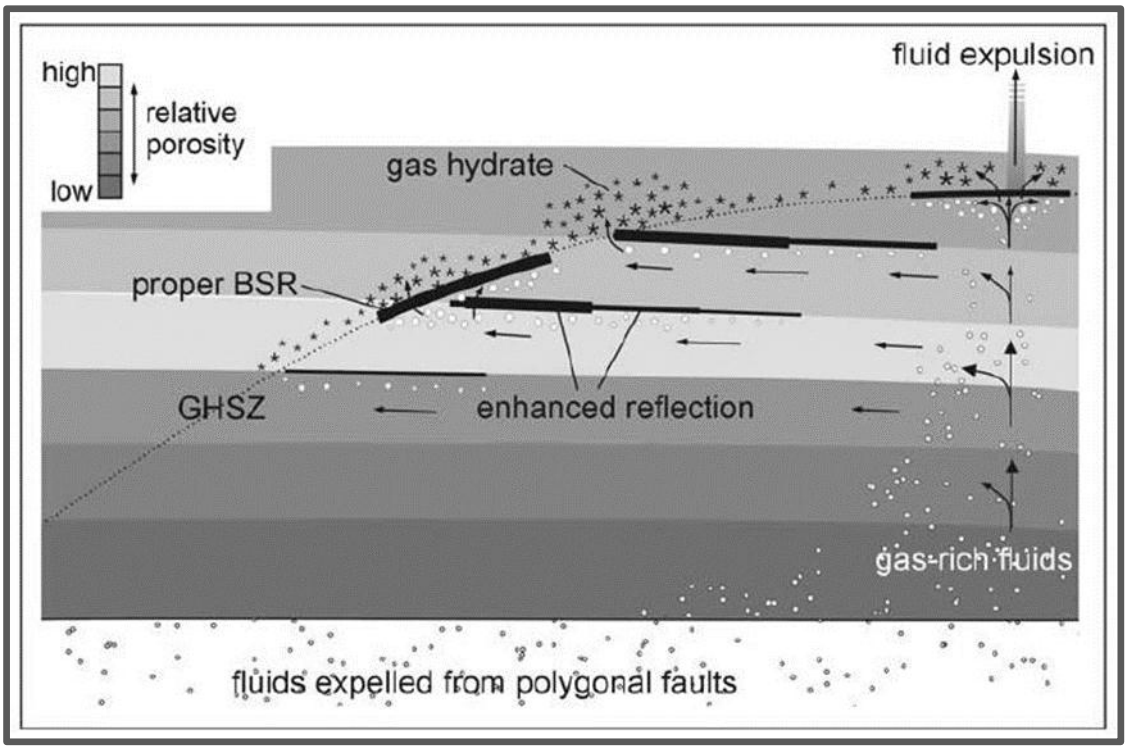

Figure 4: Schematic model for dynamic hydrate/free gas system on the northern flank of the Storegga Slide. (from Bünz and Mienert, 2004)

1.5 CONTOURITES (SEDIMENT DRIFTS)

Contourites are sediments deposited or substantially reworked by the persistent action of bottom currents (Stow et al., 2002). They cover large parts of the ocean floor and continental margins, and occur largely in continental rise to lower slope settings. The accumulation and geomorphology of contourite deposits are mainly influenced by three factors: intensity of deepwater bottom-currents, seafloor topography, and sediment supply (Faugères et al., 1993). There are three main types of contourite accumulations as proposed by Faugères et al. (2008):

- Sheeted drifts (Figure 5) or contourite sheets are characterized by a wide, mounded geometry, covering a large area with uniform thickness. The internal seismofacies is typically low-amplitude, discontinuous reflectors. They show a predominantly aggradational stacking pattern with no significant migration and may comprise or be covered by large fields of sediment waves. Three kinds of sheeted drifts are identified: (a) abyssal sheets, which cover basin plains whose margins trap the bottom currents; (b) slope sheets, which are spread out across margins where a gentle gradient and smooth topography favor a wide non-focused current; and (c) channel-related patch sheets.

- Mounded drifts (Figure 5) are characterized by their distinctly mounded and more or less elongated geometry. They commonly show good parallel to sub-parallel seismic reflectors. Three kinds of mounded drifts are identified: (a) giant elongated drifts, ranging from a few tens of kilometers to over 1000km long, thicknesses of up to several hundreds of meters, and situated parallel or sub-parallel to contours; (b) channel-related drifts, which are specifically related to narrow conduits (deep channels, gateways or contourite moats) where the bottom circulation is constrained and flow velocities increased; and (c) confined drifts deposited in relatively small confining basins.

• Mixed drift systems involve the significant interaction of contour currents with other depositional processes, and characterized by both down-slope and along-slope processes, where the normal contourite-drift morphologies and development may be markedly modified.

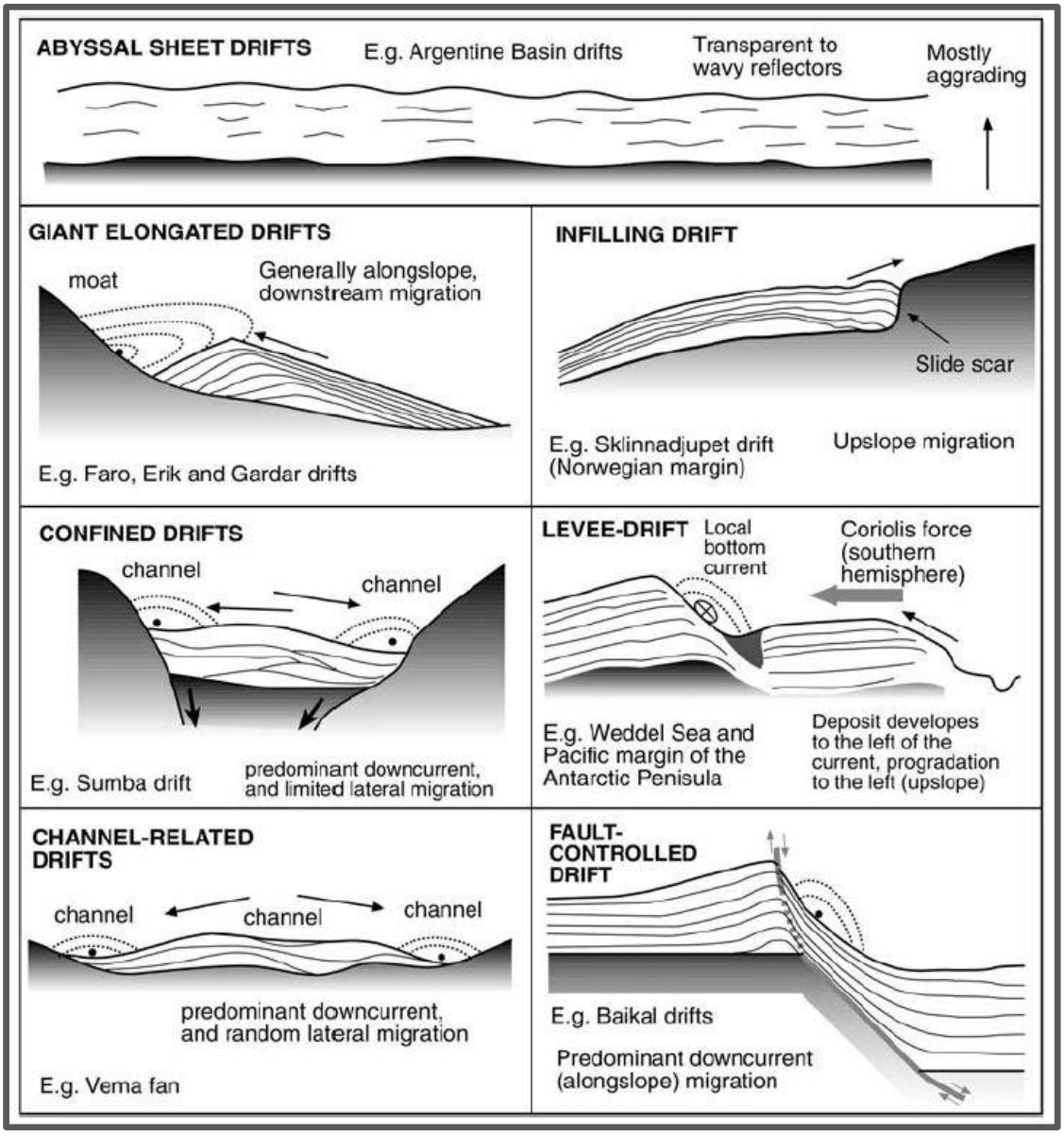

Figure 5: Summary of the different types of contourite drifts (after McCave and Tucholke, 1986; Faugères et al., 1999) showing the drift general geometry, migration trend (black arrow) and inferred axis of bottom-current flow (dashed arches). (from Rebesco and Stow, 2001)

In Northern Europe, from southwest Ireland to offshore central Norway, persistent bottom currents have generated drift deposits which mostly have elongated mounded geometries with well-layered internal acoustic signatures and composed of sandy and muddy contourites, with facies indicating that deposition was dominated by a combination of bottom currents, ice-rafting and hemipelagic settling (Hernández-Molina et al., 2008). Along the Norwegian shelf, there is present winnowing along the shelf and upper slope by the inflowing currents of the Atlantic waters, and the contourites derived from the winnowing are deposited in lower slope embayment and in slide scars (Laberg et al., 2005), whereas deep persistent currents have influenced the sedimentation in large parts of the Fram strait at the NW Svalbard margin (Eiken and Hinz, 1993).

The study of contourites has considerable impact on three research areas: hydrocarbon exploration, climate change and slope stability.

The economic significance of contourites has been recognized due to the advance of hydrocarbon exploration toward deeper waters. This demands a better understanding of the role of bottom currents and their implications for petroleum systems such as reservoir and sealing rocks. Seismic and well-log characteristics of coarse-grained contourites can reveal high reservoir potential. Fine-grained drifts can locally and regionally develop large and thick accumulations, which have an important seal potential for trapping hydrocarbon (Viana et al., 2007). It is also worth noting that along the Atlantic passive margin settings, gas hydrates associated with BSRs are mainly found in contourite deposits (Dillon and Paull, 1983). In some cases, sediment erosion by contour currents can trigger the release of methane from gas-hydrate accumulations (Holbrook et al., 2002).

2 GEOLOGICAL OVERVIEW

2.1 TECTONIC SETTING

The Svalbard archipelago is located on the north-western edge of the European continental shelf and bordered by the Arctic Ocean, Fram Strait, Norwegian and Barents Sea (Figure 6). Seafloor spreading in the Eurasian Basin and the Norwegian-Greenland Sea occurred in the early Eocene times as Greenland and North America separated from Eurasia (Demenitskaya and Karasik, 1969; Talwani and Eldholm, 1977; Eldholm et al., 1987). A rotation in spreading in the early Oligocene terminated the Western Spitsbergen Orogeny and forced rifting along the continental transform between the Barents Sea and Greenland, leading to oblique spreading along the Knipovich Ridge and finally continental separation of Greenland and Svalbard (Talwani and Eldholm, 1977; Faleide et al., 1991). After subsidence, the Fram Strait developed as the only deepwater passage to the Arctic Ocean, playing a crucial role in ocean circulation processes (Eiken and Hinz, 1993).

The forming of new oceanic crust started at about 20 Ma, with a low spreading rate (1,5-2 cm/yr), resulting in a short distance between the main spreading ridge and the continental shelf. A series of transform faults and short spreading centers connect the Knipovich Ridge in the most northern part of the Norwegian-Greenland Sea with the Gakkkel Ridge in the eastern Arctic basins (Talwani and Eldholm, 1977; Thiede et al., 1998). West dipping faults are common, formed as compressional to transpressional structures during the Western Spitsbergen Orogeny, and then extended during the opening of the ocean between Greenland and Svalbard.

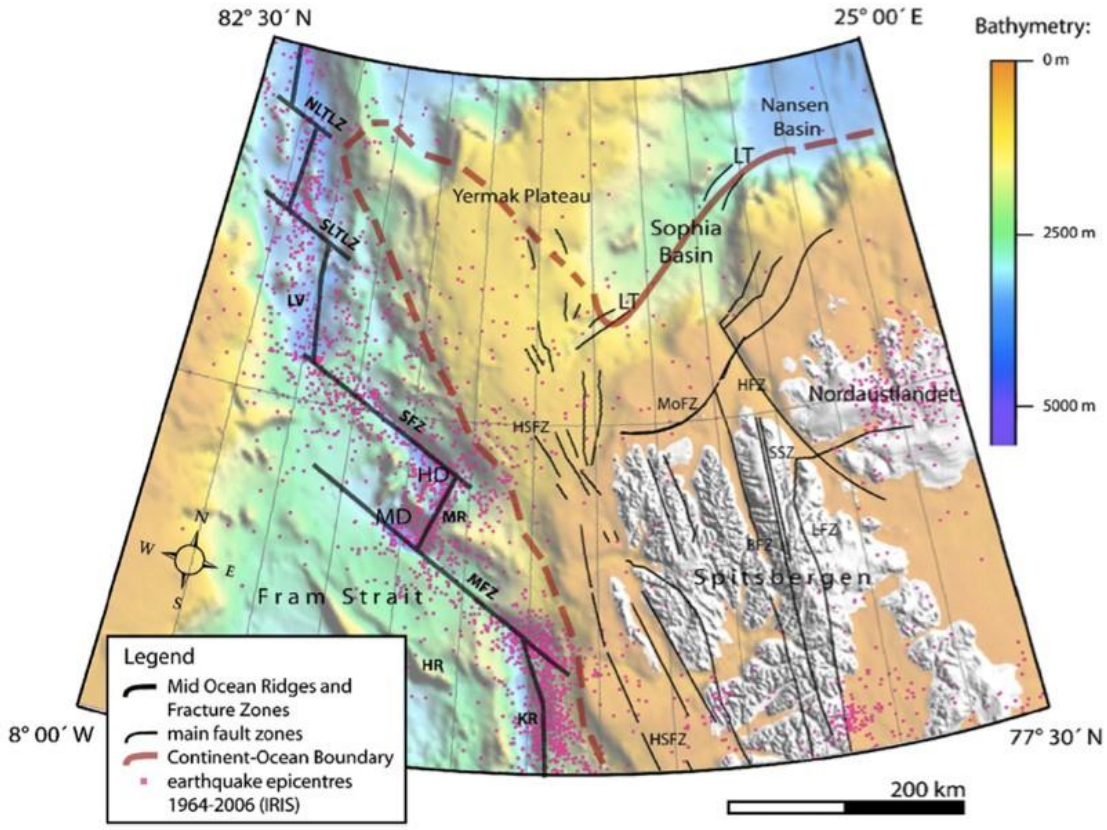

Figure 6: Structural map of the Svalbard area with plate boundaries, fracture zones and major fault zones according to various authors as cited by Winkelmann et al. (2008). BFZ – Billefjorden Fault Zone; HD – Hayes Deep; HFZ - Hinlopen Fault Zone; HR - Hovgård Ridge; HSFZ - Hornsund Fault Zone; KR - Knipovich Ridge; LFZ - Lifdefjorden Fault Zone; LT - Littke Trough; LV - Lena Valley; MD - Molly Deep; MFZ - Molly Fracture Zone; MoFZ - Moffen Fault Zone; MR - Molly Ridge; NLTFZ - North Lena Trough Fracture Zone; SFZ - Spitsbergen Fracture Zone; SLTFZ - South Lena Trough Fracture Zone. (from Winkelmann et al., 2008)

The continental margin north of Svalbard is considered to be of non-volcanic nature (Geissler and Jokat, 2004). The continent-ocean transition in the area is characterized by down-faulted basement rocks rather than by seaward dipping volcanic sequences. Some of the faults in the southern Yermak Plateau cutting through the young sediments near the seafloor, in addition to sparsely occurring earthquakes (IRIS, 2000) in the area, point to recent crustal movements, which are connected with the evolution of the plate boundary along the Spitsbergen Fracture Zone. SW-NE structures are dominant following the modern continental margin.

2.2 OCEAN CURRENTS

Svalbard is dominated by two main surface currents, the West Spitsbergen Current (WSC), a shallow northward-flowing warm water branch of the North Atlantic Current (NAC), and the cold southward-flowing East Greenland Current (EGC) (Aagaard et al., 1987). The area between these two surface currents is characterized by mixed waters (Swift and Aagaard, 1981). The relatively warm and saline incoming Atlantic Water (AW) provides major pathway for heat and water transport into the Arctic Ocean, and an integral part of the global thermohaline circulation (Ślubowska-Woldengen et al., 2007).

The Fram Strait is the 2500 m deep channel connecting the Nordic Seas to the Arctic Ocean. The North Atlantic Water (AW) flows through the strait along its eastern side as the upper 850m part of the WSC (Fahrbach et al., 2001; Schauer et al., 2004) and eventually branches out. The largest one, Knipovich Branch (KB), separates from the WSC and flows above the Knipovich ridge and the Greenland-Spitsbergen sill, and joins the East Greenland Current flowing southwards on the western side of the Fram Strait. Further north, at 79°–79°45"N, the remaining WSC splits into the Svalbard Branch (SVB) and the Yermak Plateau Branch (YPB) (Figure 7).

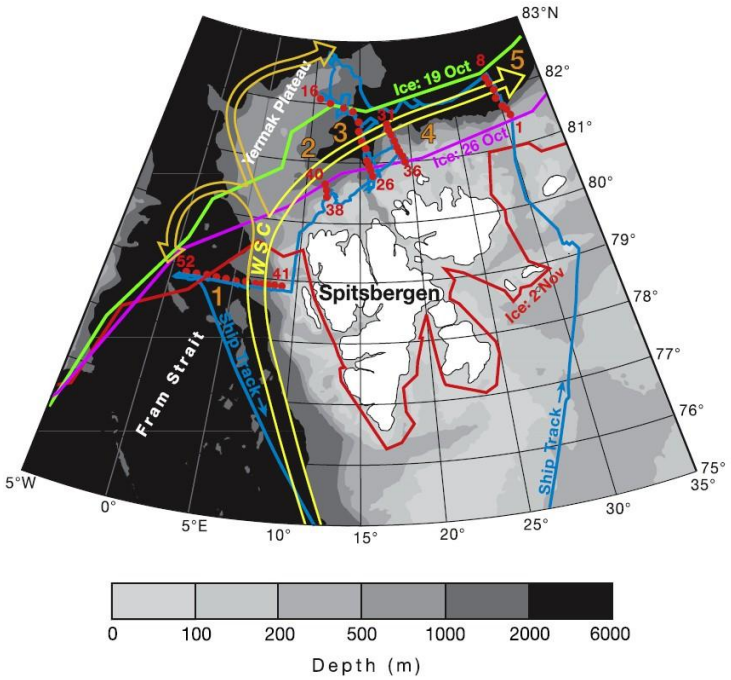

Figure 7: Map of ocean currents on the west and north of Svalbard. The path of the West Spitsbergen Current (WSC) is after Rudels et al. (2005). (from Cokelet et al., 2008)

In Fram Strait, the observed depth of the AW core is at 150–200 m and the lower boundary of the AW has been observed between 600–715 m (Schauer et al., 2004; Cokelet et al., 2008; Aksenov et al., 2010) (Figure 8). The seabed topography affects the local current pattern as the current speed intensifies with an increase in steepness of the slope (Cokelet et al., 2008) (Figure 9).

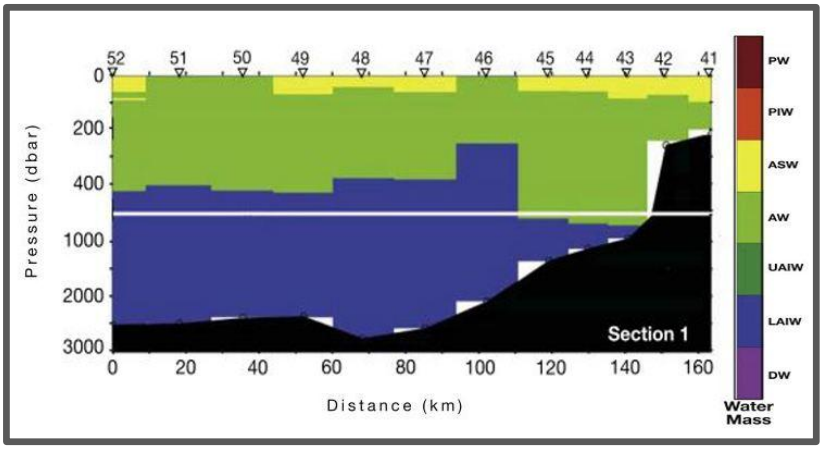

Figure 8: Water mass type for Section 1 (location on Figure 4) looking downstream in the West Spitsbergen Current, Svalbard Branch SVB, from October to November 2001. PW = Polar Water, PIW= Polar Intermediate Water, ASW = Arctic Surface Water, AW = Atlantic Water, UAIW = Upper Arctic Intermediate Water, LAIW = Lower Arctic Intermediate Water, DW = Deep Water (after Aagaard et al., 1985). (from Cokelet et al., 2008)

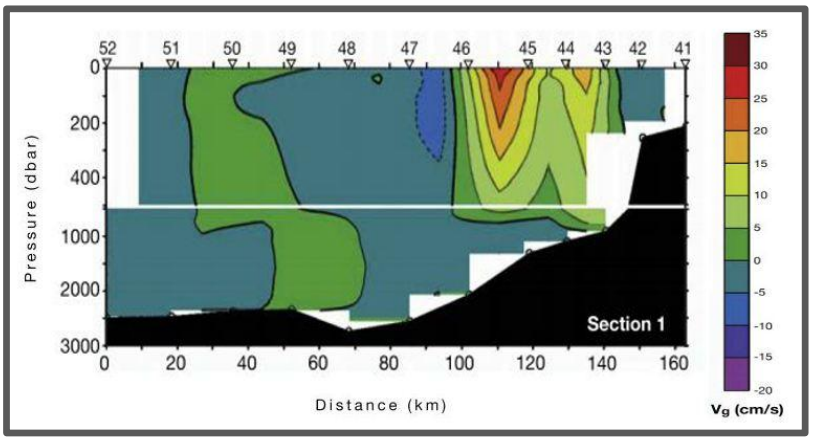

Figure 9: Geostrophic velocity for Section 1 (location on Figure 4) looking downstream in the West Spitsbergen Current, Svalbard Branch SVB, from October to November, 2001. (from Cokelet et al., 2008)

2.3 SEDIMENTATION AND SEABED MORPHOLOGY

The presence and dynamics of glaciers and ice streams during Plio-Pleistocene glaciations have had a pronounced effect on both sedimentation and erosion on the Svalbard continental margin. These fast-flowing ice streams scoured cross-shelf troughs and pushed large volumes of terrigenous sediments beyond the shelf break during glacial times, resulting in shelf progradation and stacked glacigenic debris flow deposition on the upper slopes (Ottesen et al., 2005).

The morphology of the Svalbard shelf indicates glacial activity during the Plio-Pleistocene when glaciers repeatedly reached the shelf break (Solheim et al., 1996; Solheim et al., 1998; Vorren et al., 1998), with the last three advances taking place during the Weichselian (Mangerud et al., 1998). The shelf is characterized by fjord and cross-shelf trough systems, which typically drain into trough mouth fans, separated by shallower banks (Figure 10). Submarine morphological evidence, along with stratigraphical and chronological data from previous studies (Svendsen et al., 1992 1996 2004, Andersen et al., 1996, Landvik et al., 1998, Mangerud et al., 2002) show that the Late Weichselian ice sheet reached the continental shelf edge west and north of Svalbard. This ice sheet was partitioned into fast-flowing ice streams which retreated rapidly from the cross-shelf troughs and outer fjords, separated by slower moving ice on the intervening shallower banks. Ice calving is thought to have been the main mechanism responsible for the rapid mass loss from ice sheets on the deeper cross shelf troughs (Ottesen et al., 2007a).

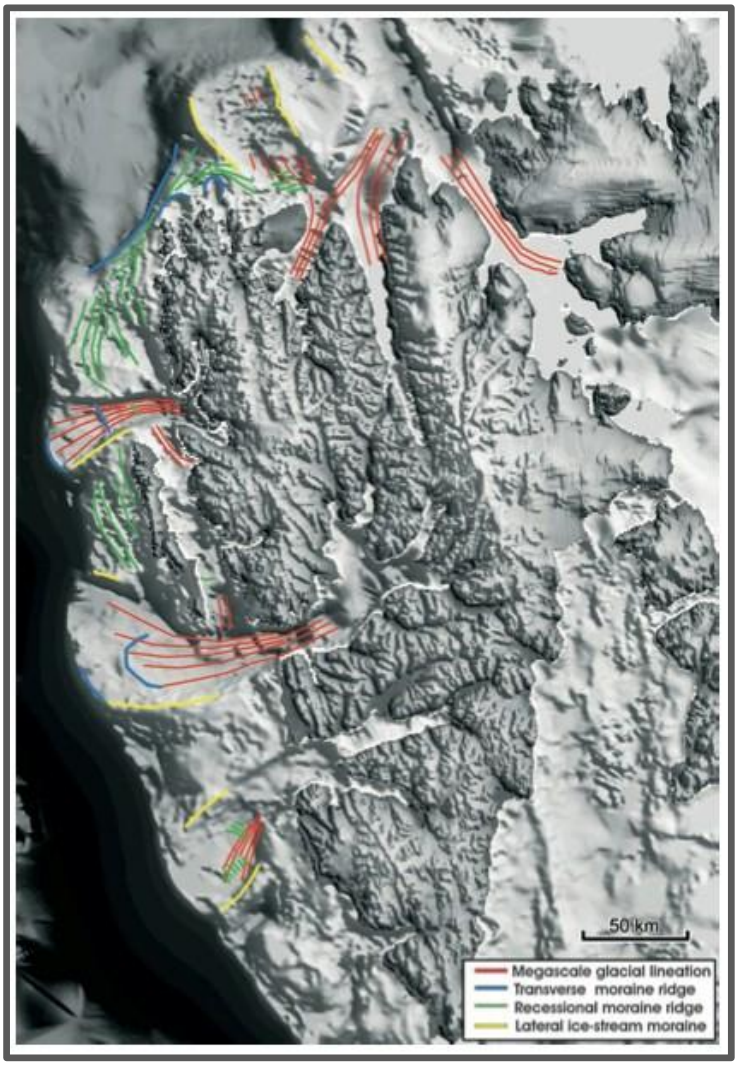

Figure 10: Geomorphic map of submarine bedforms on the Svalbard continental margin: ***Mega-scale glacial lineations*** *formed at the base of fast-flowing ice streams,* ***Transverse ridges*** *interpreted as terminal moraines;* ***Recessional transverse ridges*** *(and sedimentary wedges) making major and minor stillstands during ice retreat; and* ***Lateral moraines*** *formed at ice stream lateral margins. (from Ottesen et al., 2007a)*

According to Eiken and Hinz (1993), deep persistent currents have influenced the sedimentation in large parts of the Fram Strait since the late Miocene, where contourite deposits are mainly concentrated on the eastern part of the strait. In postglacial times, the uplift of the continental crust of Svalbard and the subsidence of the young ocean crust was most likely accompanied by increases in sediment fluxes into the eastern part of the Fram strait (Eiken and Hinz, 1993). And in regions between the trough fans, the sedimentation is controlled by alongslope currents and hemipelagic deposition producing sediment drifts and thick draped sediments (Vogt et al., 1999).

Eiken and Hinz (1993) divided the Vestnesa Ridge into three seismic sequences that make up more than 2 km of sediments. These are YP-1, YP-2 and YP-3 (Figure 11) that show continuous strata with only minor unconformities and are as follows: YP-3: Sediment depocenter with a prograding pattern at the outer shelf and a second depocenter of circular shape at the Vestnesa Ridge. YP-2: Westward-thickening wedges with a migration of the depocenter and a sequence that downlaps to the west. YP-1: Lowermost sequence YP-1 with shows a subparallel reflection pattern.

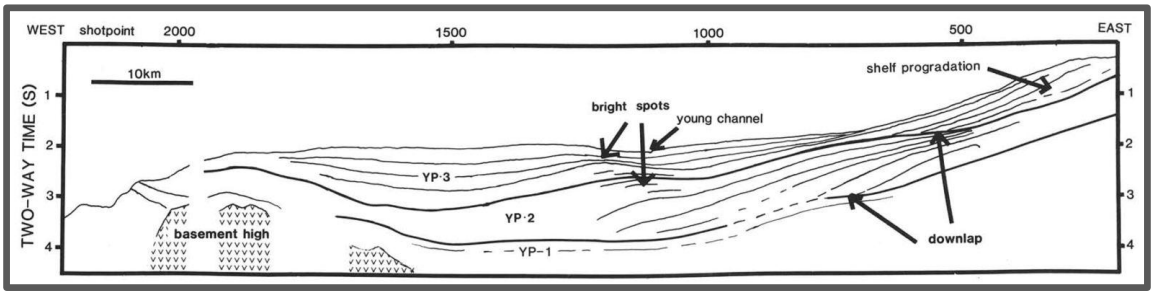

Figure 11: Interpretation of seismic line UB 18-81 parallel to Vestnesa Ridge (Eiken and Hinz, 1993).

The western Svalbard margin has been influenced by both downslope and alongslope processes (Howe et al., 2008). A sediment drift on the Vestnesa Ridge contains at least 50m of acoustically well-laminated sediments while the crest of the drift contains fine-grained silty muds. A sediment core analysis from the crest of the drift (Howe et al., 2008), suggest Holocene sedimentation dominated by muddy-silty contourite deposits from the West Spitsbergen Current, sitting above laminated silty turbidites formed from increased sediment supply and lower sea level during the LGM. The calculated high sedimentation rates of 105 cm/kyr for the pre-LGM with a decrease to less than 10 cm/kyr between the LGM and Holocene. The modern mass accumulation rates on the Vestnesa Ridge drift is at 0.12 cm/yr (Howe et al., 2008).

More recent studies (Jessen et al., 2010, Consolaro et al., 2014) looking into sediment cores from the study area describes of an upper interval of a homogenous hemipelagic grey clay (225-0 cm); a fine-grained, structureless, silty mud interval with high abundance of diatoms (335-225 cm); and a lower part with high concentration of IRD, with a greenish sandy layer (360 cm).

2.4 FLUID FLOW AT VESTNESA RIDGE

A 1-3 km wide and 50 km long pockmark field on the crest of the Vestnesa Ridge was mapped by Vogt et al (1994) using sidescan sonar. Some of the pockmarks are 100-200 m in diameter and 10-20 m deep. These pockmarks were hypothesized to have been formed by evolution of methane generated by the decomposition of marine organic matter in the sediment drift. The rising methane would collect in the ridge-crest trap, and intermittently escaping to the sea floor (Vogt et al., 1994).

Several seismic studies revealed the occurrence of a prominent bottom-simulating reflector (BSR) along the western Svalbard margin (Eiken and Hinz, 1993, Posewang and Mienert, 1999, Vanneste et al., 2005a), indicating that gas hydrates and gas accumulations are common in the area (Figure 12). The gas hydrates on the western Svalbard margin are suggested to be mainly of biogenic origin (Myhre et al., 1995, Vanneste et al., 2005b).

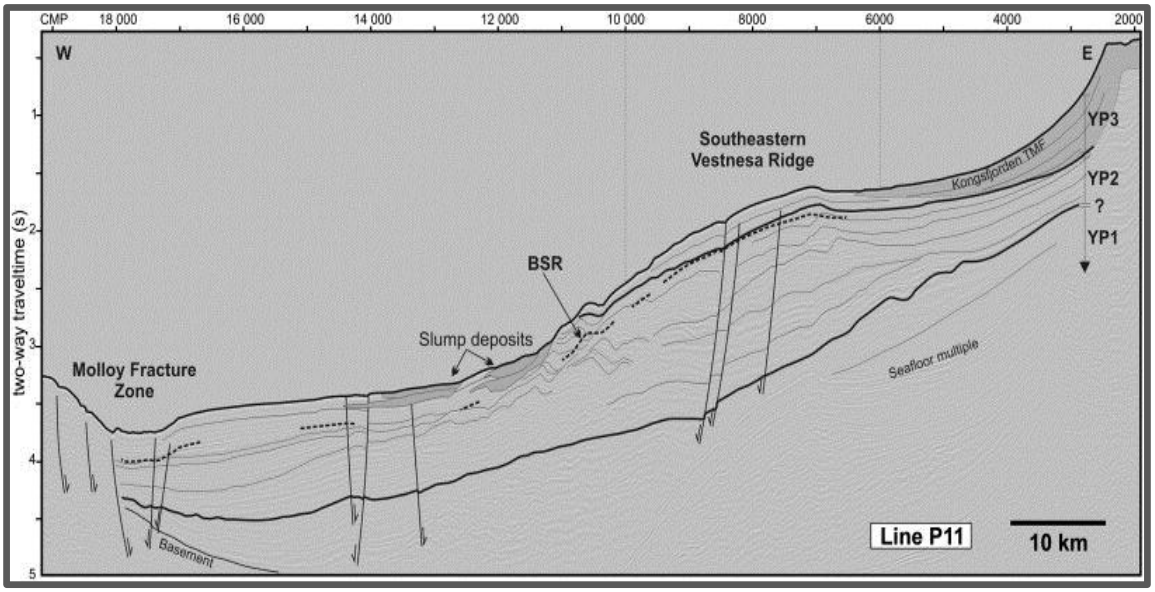

Figure 12: Multi channel seismic profile across the NW Svalbard margin from the Molloy Fracture Zone to the shelf edge and running E-W through the Vestnesa Ridge. Dashed line marks the identified BST across the margin. (from Hustoft et al., 2009)

A study in 2008 revealed a gas-hydrate, free-gas and venting system that is exceptionally more dynamic than documented elsewhere along the northeastern North Atlantic

margin (Hustoft et al., 2009). This study documented an elongated pockmark field consisting of more than 100 individual pockmarks up to 600 m wide, along the apex of the Vestnesa Ridge. Active degassing was evident from gas flares (750-m-high and 150-m-wide) observed in the water column (Figure 13). Episodic gas discharge at this site in the eastern Fram Strait has probably occurred for thousands of years, and the extensional faulting related to the Knipovich Ridge and/or thermal subsidence of the basin, may play a key role in the supply and distribution of methane hydrate and free gas across the Vestnesa Ridge (Hustoft et al., 2009).

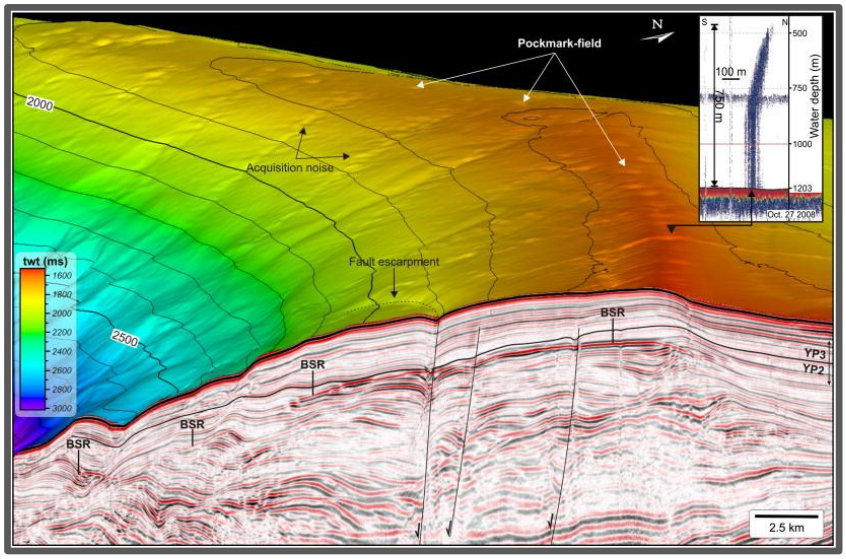

Figure 13: Swath bathymetry and profile illustrating the spatial relationship between the topography controlled pockmark field and the anticline geometry of the BSR. Inset shows echosounder data of a 750 m tall gas flare coming from a pockmark/chimney structure (from Hustoft et al., 2009).

The pockmarks at the western end of the Vestnesa Ridge were studied in detail using high-resolution 3D seismic data (Petersen et al., 2010). It was concluded that pressure-driven focused fluid flow could explain the hydro-fracturing processes that control the plumbing system and lead to extensive pockmark formation at the crest. High-amplitude anomalies in the upper 50 m of the chimney structures suggest formations of near-surface gas hydrates and/or authigenic carbonate precipitation while the deeper high-amplitude reflections above the BSR are associated with the occurrence of hydrate layers (Petersen et al., 2010).

A more recent study (Bünz et al., 2012) also used 3D high resolution seismic data to analyse the active and inactive chimney structures on the Vestnesa Ridge in further detail (Figure 14). The data indicates the presence of free gas and gas hydrate based on a strong BSR, making it one of the northernmost documented oceanic gas hydrate provinces. The focused fluid flow at the crest of the ridge suggests a strong topographically controlled fluid migration, with gas hydrates like inhibiting vertical gas flow through the flanks of the ridge (Bünz et al., 2012). The study also considers the Vestnesa Ridge as unique on Earth, due to its close proximity a mid-oceanic ridge and a transform fault, with the hydrothermal circulation system affecting the dynamics of its gas-hydrate and free-gas system.

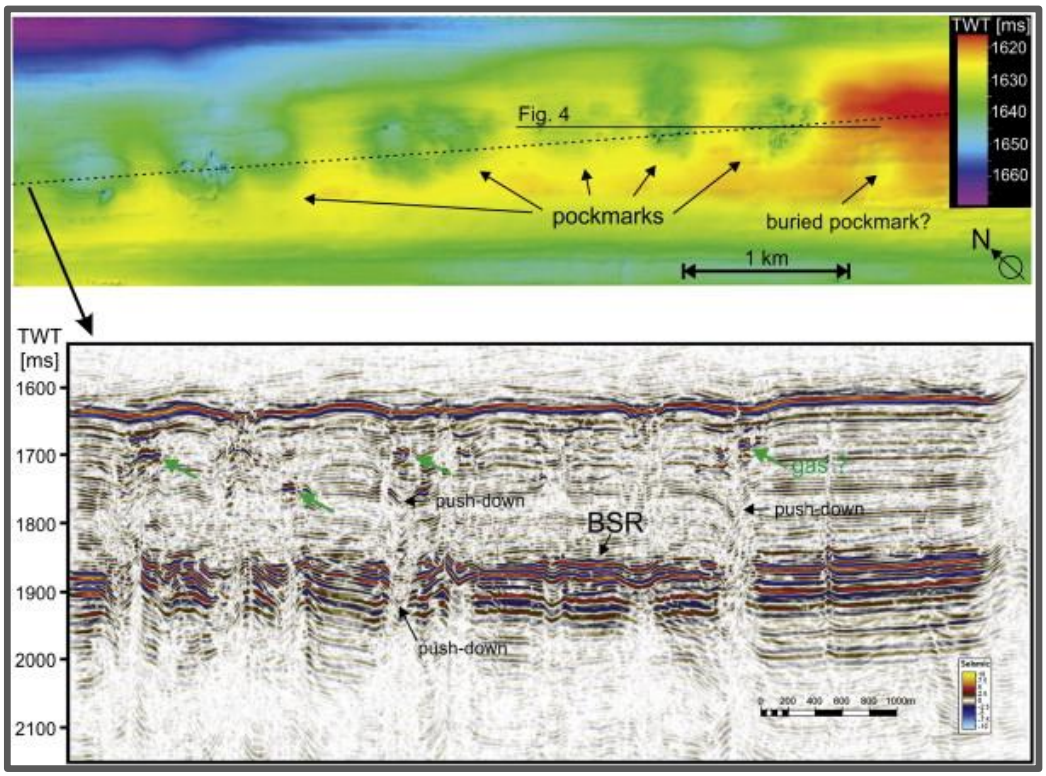

Figure 14: Top: 3D seismic interpretation of the seafloor showing pockmarks. Bottom: Seismic line showing fluid flow structures (shimneys) associated with the individual pockmarks. (from Bünz et al., 2012)

The active gas leakage at the eastern part of the Vestnesa Ridge on the upper continental slope is more extensive than previously assumed (Bünz et al., 2012). The seeps showed continuous gas leakage during survey cruises in 2010 and 2012. In 2010, the highest flare reached a height of 930 m (270 mbsl). In 2012, the highest flare reached a height of 990 m (210 mbsl) (Figure 15). These flare heights suggest that hydrate skins are developing around the bubbles, decreasing gas-dissolution processes during bubble rise and allowing bubbles to reach such heights (Smith et al., 2014). Geochemical analyses from the area also show that a thermogenic source is supplying methane and other light hydrocarbons to the Vestnesa Ridge (Smith et al., 2014) .

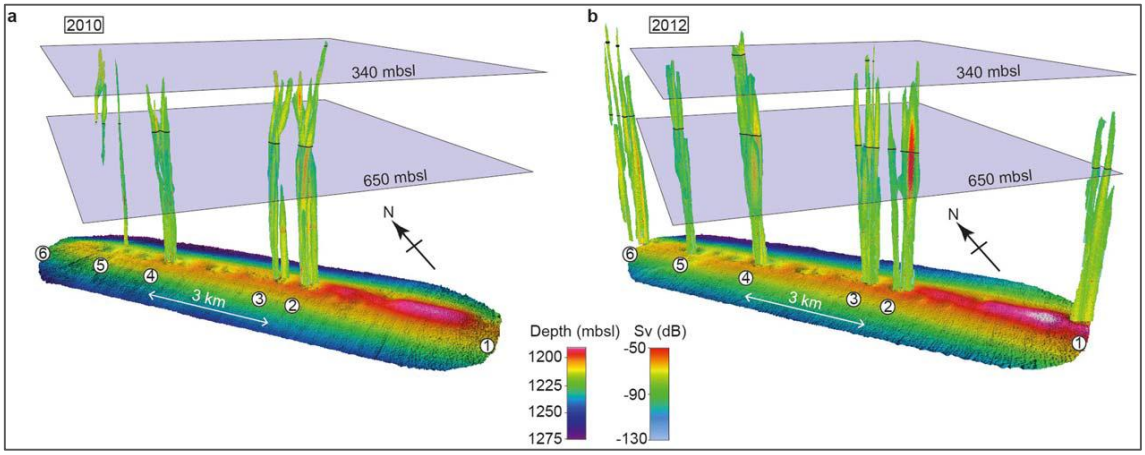

Figure 15: Flares above pockmarks at the Vestnesa Ridge in (a) 2010 and (b) 2012. (from Smith et al., 2014)

3 MATERIALS AND METHODS

3.1 KONGSBERG-SIMRAD EM300 MULTIBEAM SONAR SYSTEM

The EM 300 multibeam echosounder (Figure 16) is designed to do seafloor mapping from 10m depth down to more than 5000m depth with swath widths up to about 5000m. It includes sensor interfaces, data displays for quality control and sensor calibration, seabed visualization, and data logging, as well as integrated seabed acoustic imaging capability.

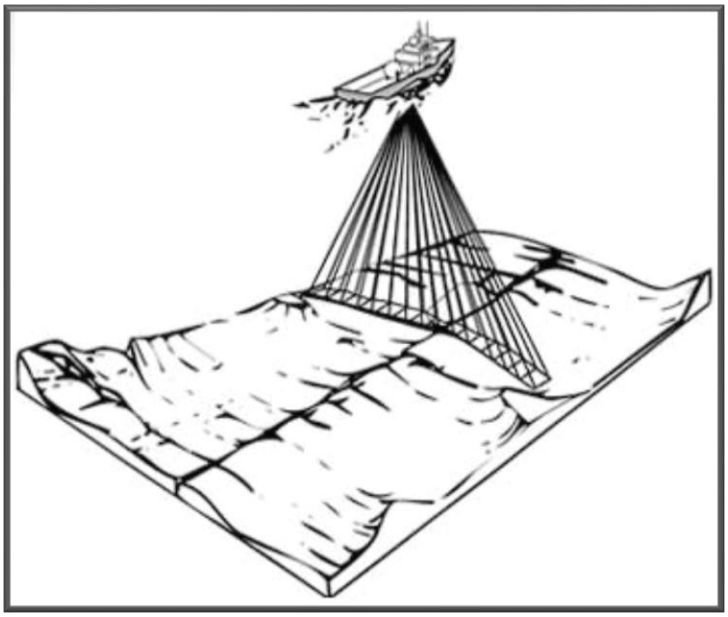

Figure 16: Diagram of multibeam sonar scho sounding the seafloor. The sonar illuminates narrow swath elongated across the bottom and perpendicular to the path of the boat. (from www.oicinc.com/multibeam.html)

The nominal sonar frequency is 30 kHz with an angular coverage sector of up to 150 degrees and 135 beams per ping as narrow as 1 degree. On a flat bottom, the swath width is normally up to 5.5 times the water depth. The number of beams can be maximized by setting the angular coverage sector and beam pointing angles to vary according to the achievable coverage.

The soundings are fit to a line perpendicular to the survey line, which ensures a uniform 100% sampling coverage. This transmit fan is split in sectors which are frequency coded (30 to 34 kHz). These sectors are all transmitted sequentially at each ping. Sector steering, refraction due to the sound speed profile, vessel attitudes and installation angles are taken into account when the sounding position and depth is calculated, while pulse length and range sampling rate are variable with depth. The ping rate is mainly limited by the round trip travel time in the water up to a ping rate of 10 Hz.

The EM 300 transducers are linear arrays with separate units for transmit and receive (

Table 1). The arrays are divided into modules with 1 and 2 degrees beamwidths as a standard. 4 degrees beamwidth is available for the receive array, with resulting array lengths of 0.8 to 3.3 m.

Main operational frequency	30 kHz	Frequencies in the range of 30 to 34 kHz are employed to code the different transmit sectorsNumber of beams for each ping: 135
Beamwidths	1x1, 1x2, 2x2 or 2x4 degrees	Other beamwidth cobinations are possible in accordance with the number of transducer modules installed
Beam spacing	Equidistant or equiangle	
Coverage sector	Up to 150 degrees	
Transmit beam steering	Stablized for roll, pitch and yaw	
Receive beam steering	Stabilized for roll	
Maximum ping rate	10 Hz	
Depth range from transducers	10 to 5,000 m	
Depth resolution	1 to 16 m	
Pulse lengths	0.7, 2, 5 and 15 ms	
Range sampling rate	4.5 kHz (17 m)	

Table 1: Technical specifications of the multibeam echosounder. (adapted from Kongsberg Technical Manual 2004)

Beams are converted into water depth on-site, using accurate sound velocities through the water column, as measured from CTD (conductivity-temperature-depth recorders) profiles of sound velocity during the survey, after appropriate filtering and editing. These profiles record the changing speed of the acoustic pulses with water salinity, temperature and depths. The Simrad processors use the sound speed data for instantaneous beam forming and ray tracing of each individual beam, at the same time as they correct for the vessel attitude. The result is the conversion of range and angle data to xyz triplets. A graphical user interface provides control on the data quality and runtime parameters used during acquisition.

3.1 BATHYMETRIC PROCESSING AND 3D VISUALIZATION

Data processing consisted of cleaning and filtering navigation data, noise reduction, data editing and visualization using the QPS Fledermaus software package Pro version 7. Fledermaus is a set of interactive 3D visualization tools for data preparation, analysis and presentation. It allows for assembling and exploring a virtual 3D of object models including surfaces, images, points, lines, and cross-sections, and is tailored for the display of geographic data such as digital terrain models of the ocean floor or a 3D contour map of a mountain range. The software allows for import of a wide variety of data formats, making it possible for producing combined 3D models. Two specific programs were utilized for the bathymetric data: Fledermaus, which is the main interactive 3D exploration application, and DMagic, the data preparation tool.

The multibeam echosounder data files (.all format) contain a series of datagrams: Water column, Position and Heading. The data were gridded, and outliers were identified, flagged, deleted in DMagic, resulting in a relatively noise-free grid. The most important parameter when gridding data is the cell size, which determines the dimensions of the surface to be created. These dimensions are determined by taking the range of the input data in the X and Y dimensions, dividing it by the cell size, and rounding up. When gridding, the number of neighboring soundings inside a given radius is important – a too small radius may not reduce noise from the data, and a too large radius might smooth

out the surface characteristics. There are three types of surfaces that can be used from irregularly spaced XYZ data:

- Weighted Moving Average – default weighted average algorithm
- Shallow Biased – minimum value in the cell
- Median Filtered – median value in the cell

The gridding algorithm allows each grid cell to blend slightly with neighboring grid cells. The amount that a given point contributes to any cell falls off linearly with distance from the point's location. The Weight Diameter determines how many cells the area of effect will extend over. A value of one will force the point to affect only the cell that contains it, while a value of three will affect the contained cell and all eight neighboring cells. A value of five extends the effect to the neighbors' neighbors. Only odd numbers for the weight field diameter are used. The Weight Diameter is not relevant when using Shallow Biased or Median Filtered gridding.

3.2 BACKSCATTER PROCESSING AND VISUALIZATION

Backscatter strength is the intensity of the acoustic response, corresponding to the relative amount of energy sent back from target, measured in decibels. The backscatter strength depends on the physical nature of the seafloor, structure and the frequency and angle used. Acoustic backscatter data are often useful for classifying seafloor characteristics (Lurton, 2002).

Backscattering is affected by three factors: geometry of the sensor-target system (local slope, local angle of incidence, etc.), the physical characteristics of the surface (roughness, sound speed, etc.) and the intrinsic nature of the surface (composition, density, etc.) (Figure 17). Slopes facing toward the sonar will produce more backscatter and a rougher surface will produce more backscatter. The effect of volume scattering should also be taken into account due to a possible acoustic penetration at the frequency used (Blondel, 2009).

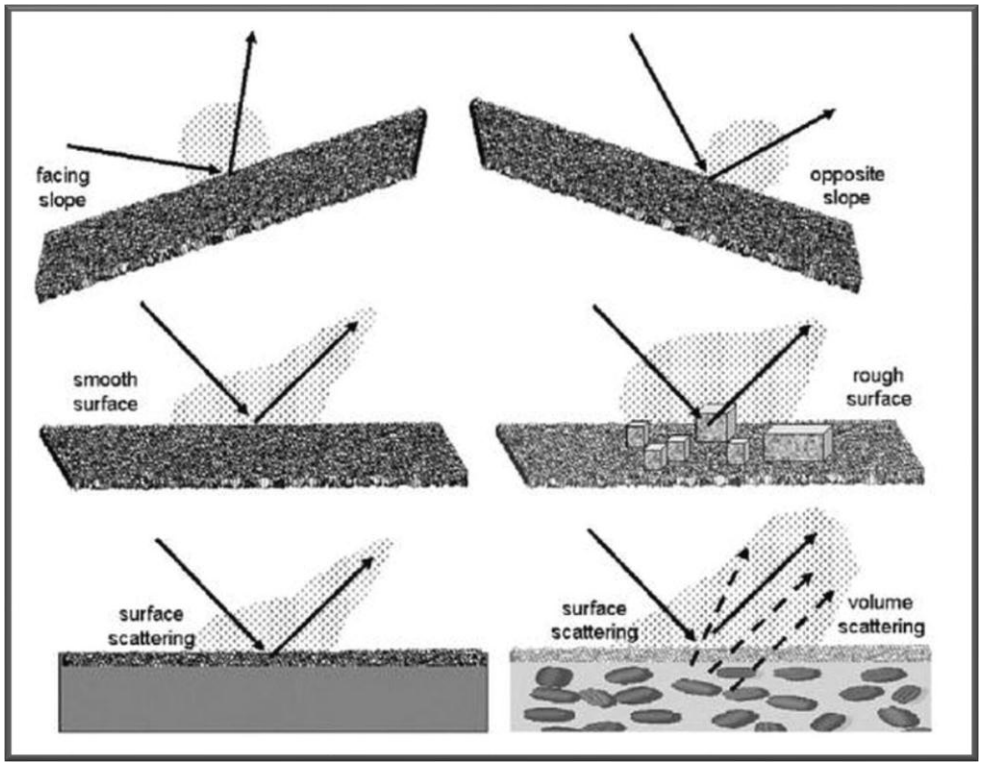

Figure 17: Backscattering from the seafloor is influenced by three factors: A) local geometry of area of ensonification, B) roughness of the seafloor at scales comparable to the sonar's wavelength, C) intrinsic properties of the seafloor (e.g., rocks vs. sediments). (from Blondel, 2009).

Backscatter strengths describe the response of the seafloor at the frequency used and for specific conditions of ensonification (mostly the grazing angle). If calibrated and expressed in dB, they can also be compared with acoustic backscatter models, providing more insights into seafloor processes. Full knowledge of the processing chain and the accuracy of the calibrated backscatter strength of a particular pixel on the seabed, allows the interpreter to assess whether surface or volume processes predominate, and compare the geotechnical properties of this portion of the seabed with known quantities. (Blondel, 2009)

A study by Johnson et al. (2003) looked into backscatter data in determining the spatial distribution of cold seep carbonates and their relationship to subsurface structure and the underlying gas hydrate system. High backscatter data was divided into three categories (Figure 18):

• Category I - Circular to blotchy with apparent surface roughness. High backscatter due to presence of gas hydrates and authigenic carbonate.
• Category II - Circular to blotchy with no apparent surface roughness. High backscatter due likely to authigenic carbonate, with some gas hydrate, slightly buried by hemipelagic sediments.
• Category III - Streaky to continuous with variable surface roughness. High to moderate backscatter that coincides with regions of high slope angles, likely derived from deep-seated fluids but unrelated to destabilization of gas hydrate.

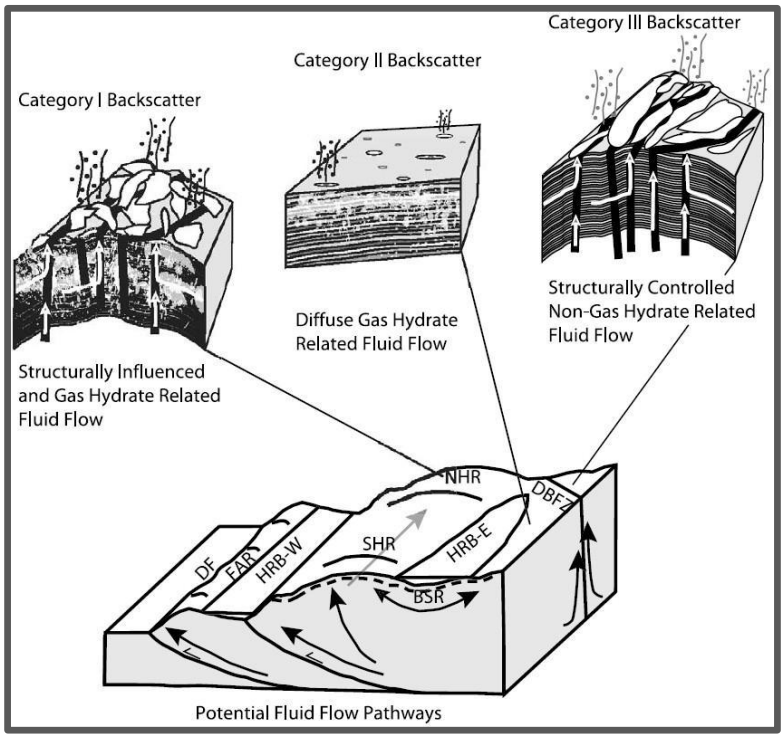

Figure 18: Schematic diagrams depicting environments likely responsible for each of the classified backscatter categories from a study of the Hydrate Ridge region offshore Oregon. (from Johnson et al., 2003)

The Fledermaus Geocoder Toolbox (FMGT) is used to process backscatter data in this study. FMGT is a software program designed to visualize and analyse backscatter data from multibeam sonars. In processing the source files into mosaics, it is designed to perform as many corrections as possible to maximize the information content within the backscatter signals. The software can read multiple files of backscatter data, apply corrections, and then create a 2D representation of the ocean floor called a backscatter mosaic. Once the mosaic has been generated, various statistics can be calculated and exported along with the backscatter in a number of different formats. Angle range analysis (ARA) can also be performed to attempt to classify the bottom types.

3.3 MULTIBEAM DATA

Swath bathymetry and backscatter data were acquired using the Kongsberg Simrad EM300 system during surveys in 2010 on R/V Jan Mayen, in 2012 and 2013 on R/V Helmer Hanssen. The system operates at a sonar frequency of 30 kHz with an angular coverage of 135^{o}. Sound velocity profiles for calibration of beams in the water column were extracted from CTD stations acquired during the surveys.

Approximately 40 km^2 of swath bathymetry data were acquired on the southeastern flank of the Vestnesa Ridge with a height range of –1190 m to –1290 m, located at 79^{o} N and 7^{o} E. Bathymetry data were gridded, plotted, cleaned, filtered and visualized using QPS Fledermaus software. Backscatter data was processed using QPS FM Geocoder Toolbox.

4 RESULTS

4.1 SWATH BATHYMETRY

4.1.1 GENERAL DESCRIPTION

The Vestnesa Ridge is a SE-NW to E-W bending elongated sediment drift situated at 79° N to the northeast of the Molloy transform fault and to the north of the Knipovich Ridge (Figure 19). At a water depth of 1200m, the ridge is situated between the Kongsfjorden Trough mouth fan in the east and the Molloy Ridge to its west. The Vestnesa Ridge is approximately 100 km long and 2.5 to 3.5 km long. The ridge widens from southeast until it bends towards the west, where it gradually starts to get narrower further westward. The mean slope angle of the Vestnesa Ridge is 0.1° from southeast until it turns westward where the slope angle gradually increases until it rapidly increases to 6° at the most western part of the ridge (Bünz et al., 2012).

More than 100 pockmarks have been identified situated on the crest of the Vestnesa Ridge. The interpreted pockmarks are seafloor depressions that have circular to oval shapes and are typical seabed expressions of fluid flow (Judd and Hovland, 2007) and are indicative of recent fluid flow activity at the crest (Hustoft et al., 2009). Pockmarks are present all along the ridge but vary in distribution and morphology along the crest. On the western part where the crest gets wider, the pockmarks are distributed over a wider area. On the southeastern part of the Vestnesa Ridge, where the crest is narrower, the pockmarks line up perfectly along the apex of the crest and are predominantly circular to elongate in shape. The pockmarks on the southeastern side of Vestnesa Ridge appear to be more numerous and larger compared to the western part. No fluid flow features have been observed on the flanks of the ridge, suggesting a strong topographically controlled migration of fluids (Bünz et al., 2012).

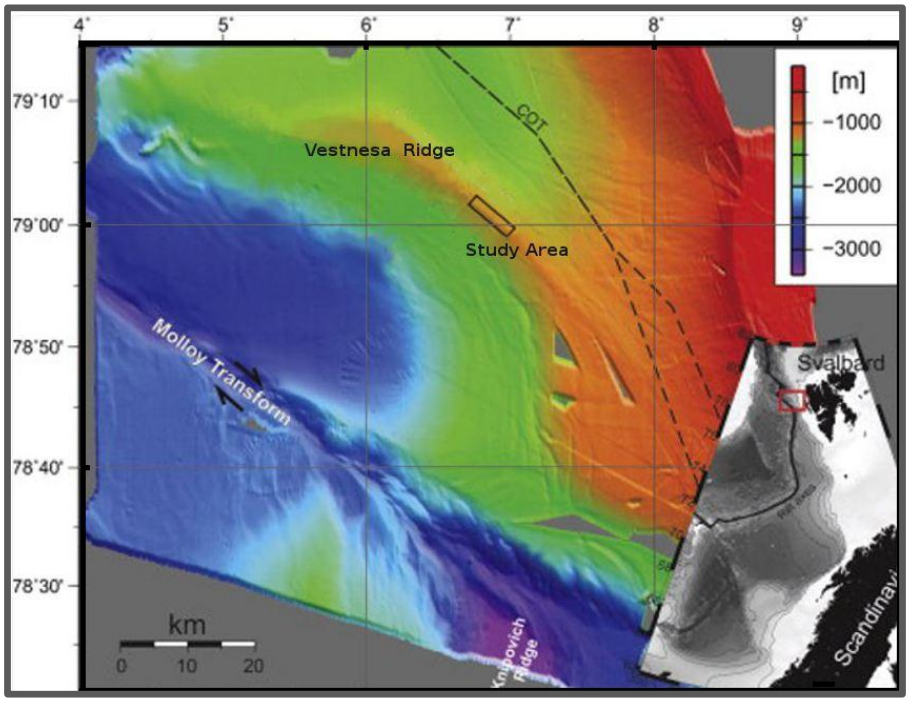

Figure 19: Location map of the study area on the Vestnesa Ridge. (modified from Bünz et al., 2012)

This study will focus on the seabed features along the southeastern part of the Vestnesa Ridge (Figure 19), where the pockmarks are larger more evenly distributed. Datasets from three different surveys in 2010, 2012 and 2013 will be compared as to account for changes in morphology over time. The datasets were gridded to 10m using the WGS 84 UTM zone 32N coordinate system, cleaned, distance-filtered and visualized on the QPS Fledermaus software (Figure 20).

The swath bathymetry covers an area approximately 42 km^2, 12 km long and 3.5 wide. The mean slope is 0.1^o from southeast to northwest along the length of the crest, with the highest part on the south-eastern end at -1190 mbsl. The mean slope from the ridge crest to southwest is 1.5^o while it is approximately 1.7^o on the other side of the crest to the northeast.

The ridge crest is interspersed by several large pockmarks that are circular to oval in shape and are close to one another that some appear as one pockmark. Some appear to have hummocky or mounded texture within. The pockmarks can reach up to 10m deep and 700m across.

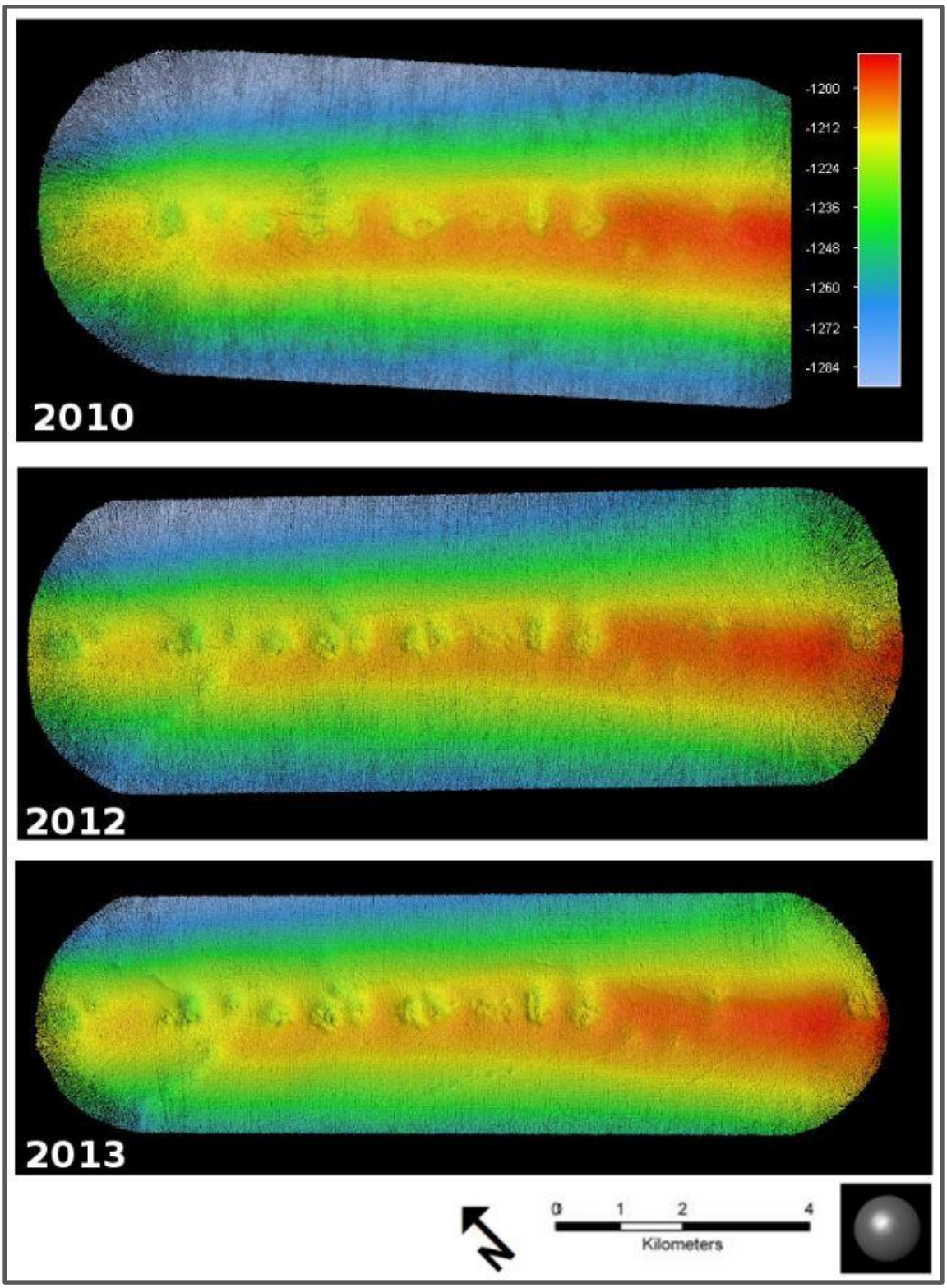

Figure 20: Swath bathymetry of the study area gridded to 10 m, from three surveys in 2010, 2012 and 2013.

4.1.2 PROFILING

Morphological changes along the ridge crest can be determined from comparing profiles of the different datasets along the same profiler plane (Figure 21). Special interest is given to specific pockmarks that have recently been observed to be actively releasing gas into the water column (Hustoft et al., 2009, Bünz et al., 2012, Smith et al., 2014). These active pockmarks are marked with red arrows on Figure 21.

The profile across the dataset is approximately 6.8 km long and goes through the evenly distributed pockmarks that are up to 700m wide and 10m deep. Changes can be detected from the shapes of the pockmark profiles, otherwise the general morphology remains more or less the same.

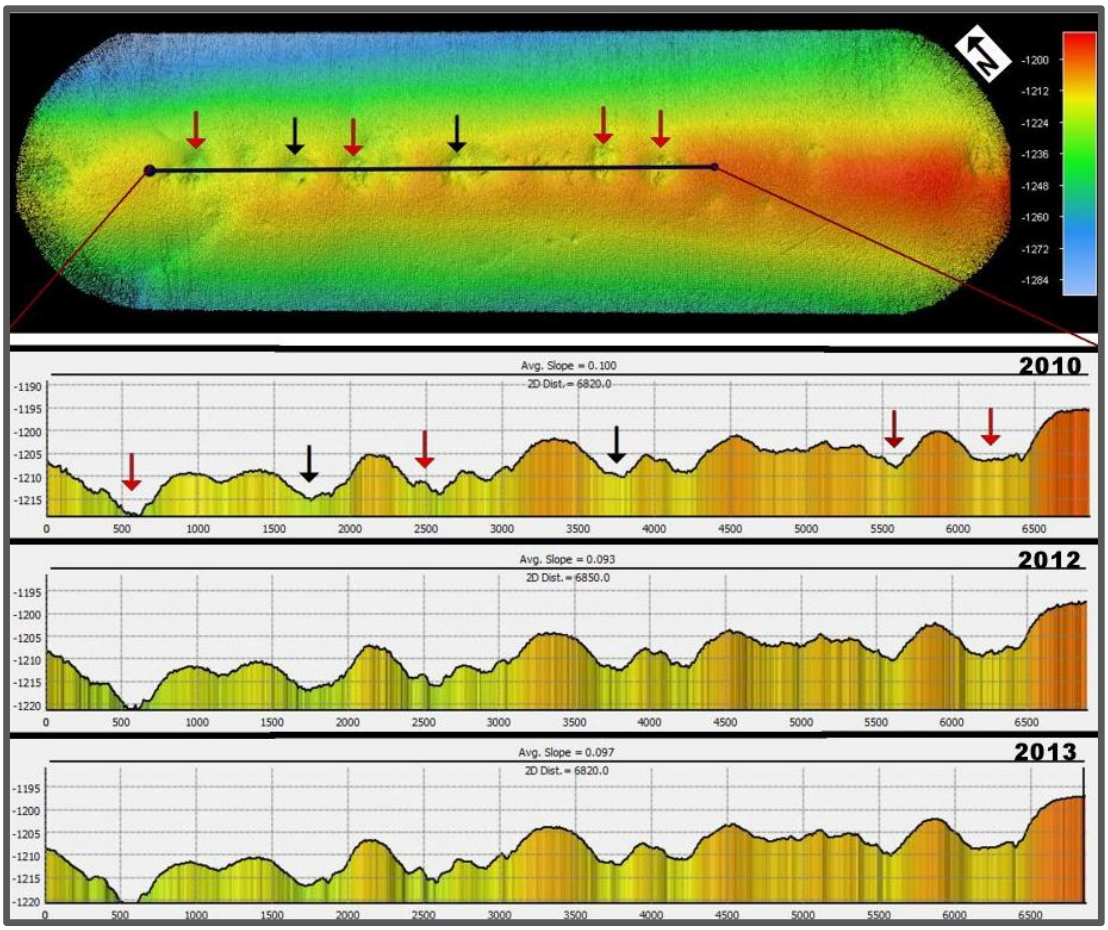

Figure 21: Profiles across the three different surveys intersecting data on the same plane. The red arrows indicate pockmarks observed to be active recently.

Superimposing the different profiles gives more information on the changes along the ridge crest. The 2010 survey is seen to be offset by about 2-3m and thus cannot be used in comparative calculations such as surface difference and volumetric changes. The offset might have been caused by recalibration of the multibeam echosounder for yaw, pitch, heave and roll, or different sets of parameters logged in the system.

Nevertheless, the 2012 and 2013 survey datasets are compatible and will be used for comparative study. In Figure 22, the 2013 profile shows to be generally higher by up to 1 m in relation to the 2012 profile, indicating deposition of sediments. In some areas, especially where the pockmarks are, there appears to be no difference and in some parts, the 2013 profile is lower than that of 2012, which could indicate erosional processes in the pockmarks. There also appears to be differences in the shapes of some of these individual pockmarks, signifying recent activity or processes that alter the surface morphology inside these pockmarks.

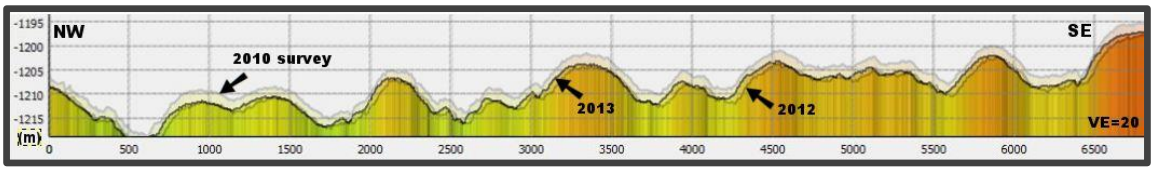

Figure 22: Profile overlay for comparison of different surveys. The 2010 survey is anomalously elevated while the 2012 and 2013 data are more compatible for comparative study.

4.1.3 CONTOURING

Contour mapping is one way of determining changes in elevation resulting from depositional or erosional processes, as well as changes in relative slope of the surface. At 10m contours, the 2012 and 2013 maps show very slight differences but generally follow the same contours (Figure 23, upper). At 2m contours, there are more marked differences at the crest. While the flanks show evenly spaced contours indicating a relatively smooth and undisturbed slope, the contours on the crest show the basins corresponding to the pockmarks, and are very uneven. It is at the crest where the two contours from 2013 and 2012 show marked differences (Figure 23, lower), indicating dynamic changes in and around the pockmarks in a span of one year. In basins where the 2013 contours enclose a 2012 contour (blue outside, red inside) could indicate deposition while 2012 enclosing a 2013 contour (red outside, blue inside) could indicate erosional processes.

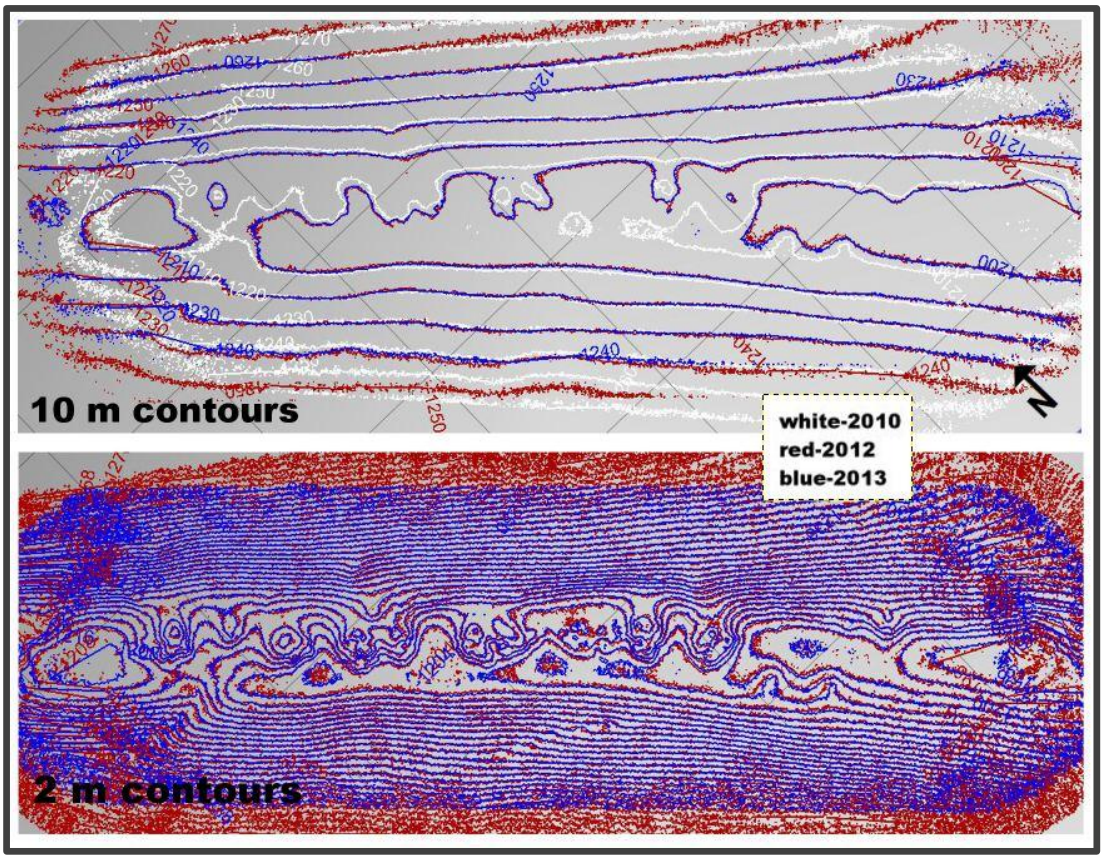

Figure 23: 10 m and 2 m contours showing smooth and even slopes on the flanks, and an uneven ridge crest. The 2 m contours of the 2012 and 2013 datasets show changes on the crest where the pockmarks are.

4.1.4 SURFACE DIFFERENCE

Calculating for surface difference, and effectively, the volume change, is another good way of determining changes in a depositional environment. In calculating for surface difference, a query is applied to the common intersection area of two input surfaces. A polygon can be used to constrain the query scope within a certain area, and can be selected to account for positive changes or negative changes in relation to the base surface, which is usually the older surface. This can be a very good tool for individually calculating volume changes in each area covered by the pockmarks.

In determining surface changes for the 2013 and 2012 surveys, the reference surface of 2012 was subtracted from the 2013 surface and surface objects were plotted as results. Figure 24 shows these two surface objects, the first is a plot of the data above the reference 2012 surface and the second is a plot of the data below the reference 2012 surface. The resulting plots show positive changes after 2012 along the crest of the ridge, indicating deposition in most parts, while areas with pockmarks show negative changes, indicating removal of sediments.

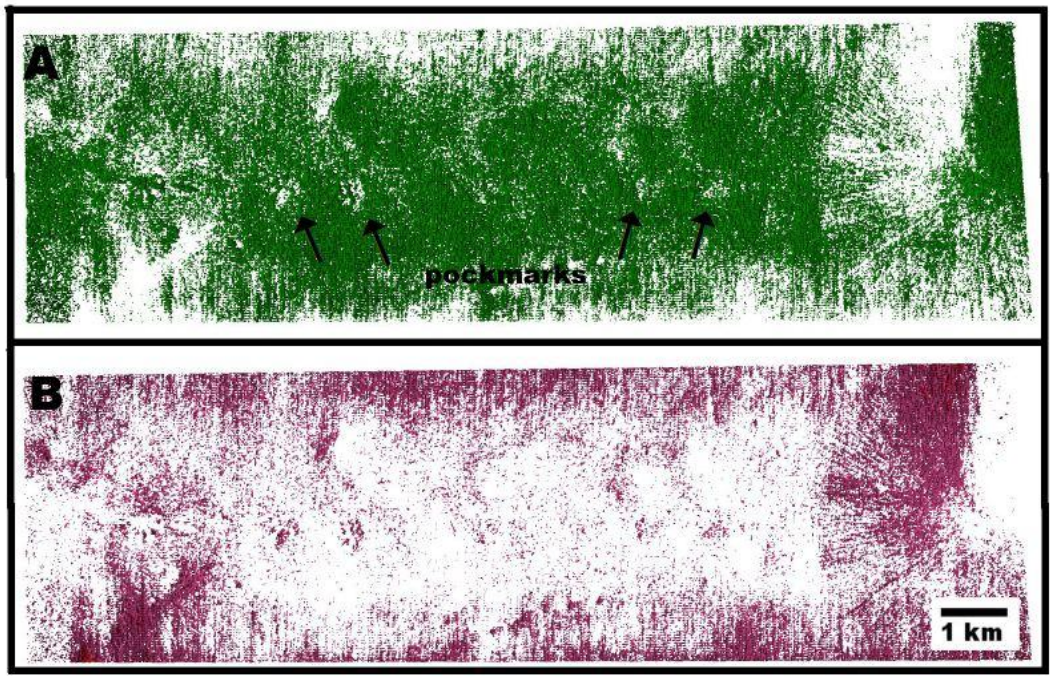

Figure 24: Surface difference plots for the 2012 and 2013 datasets. The base 2012 surface is subtracted from the newer 2013 surface. (A) Positive difference. (B) Negative difference. The patches on (A) where there is was no inferred net deposition are pockmark locations.

4.2 BACKSCATTER IMAGING

4.2.1 BACKSCATTER IMAGE OF STUDY AREA

Backscatter intensity is a function of the angle of incidence of each beam, the physical characteristics of the surface, the intrinsic nature of the surface and to some extent, the frequency and pulse characteristics of the sonar (Blondel and Murton, 1997). One of the important effects on the backscatter signal received is the effect due to bathymetric slope. Steep seafloor bathymetry sloping toward a passing sonar has enhanced backscatter strength compared to those slopes dipping away from the sonar. For the study area on the Vestnesa Ridge, the slope across the survey is 0.1^{o} which implies a high backscatter to be more likely related to changes in rock and sediment composition on the seafloor rather than a bathymetric effect. In effect, the presence of backscatter anomalies in the data would indicate a change in the physical properties of the seafloor or near sub-surface.

The resulting mosaics of the 2013 survey were gridded at 25m and 10m pixels as presented on Figure 25 and Figure 26. The maximum resolution from the data is 25m but gridding it to 10m allows for better contrast, nonetheless no additional information or details are discernible in gridding it down. Figure 25 is a backscatter mosaic of all the lines surveyed on top of the crest. They are overlapping so that the seafloor was imaged multiple times, with insonification from opposing directions. There is no data recovery directly beneath the trackline (nadir) so the resulting image are the overlapped images from the neighbouring tracks. The km wide swaths over the crest were towed NW-SE along the axis of the ridge.

Figure 26 shows another mosaic using one continuous line of swaths for imaging. The lines along the center of the trackline are also nadirs with no data recovery. The backscatter values range from -30 (low) to -19 (high) dB. The backscatter data show predominantly high-to-medium backscatter strength with a mottled texture on the gently dipping (0.1^{o}) seafloor, especially on the flanks of the ridge where the values appear similar. The backscatter on the crest are more varied. Examination of the survey

mosaic on the crest reveals some high (bright) and low (dark) backscatter spots, with the rest of the image in varying shades of grey. The low backscatter spots directly corresponds to the sites where the pockmarks are situated on the ridge crest. Inside these low backscatter spots are relatively brighter patches that corresponds to physical mounds inside the pockmarks as visible on the bathymetry. This can possibly be from the hummocky sediments or even hydrate/carbonate patches in and around the pockmarks.

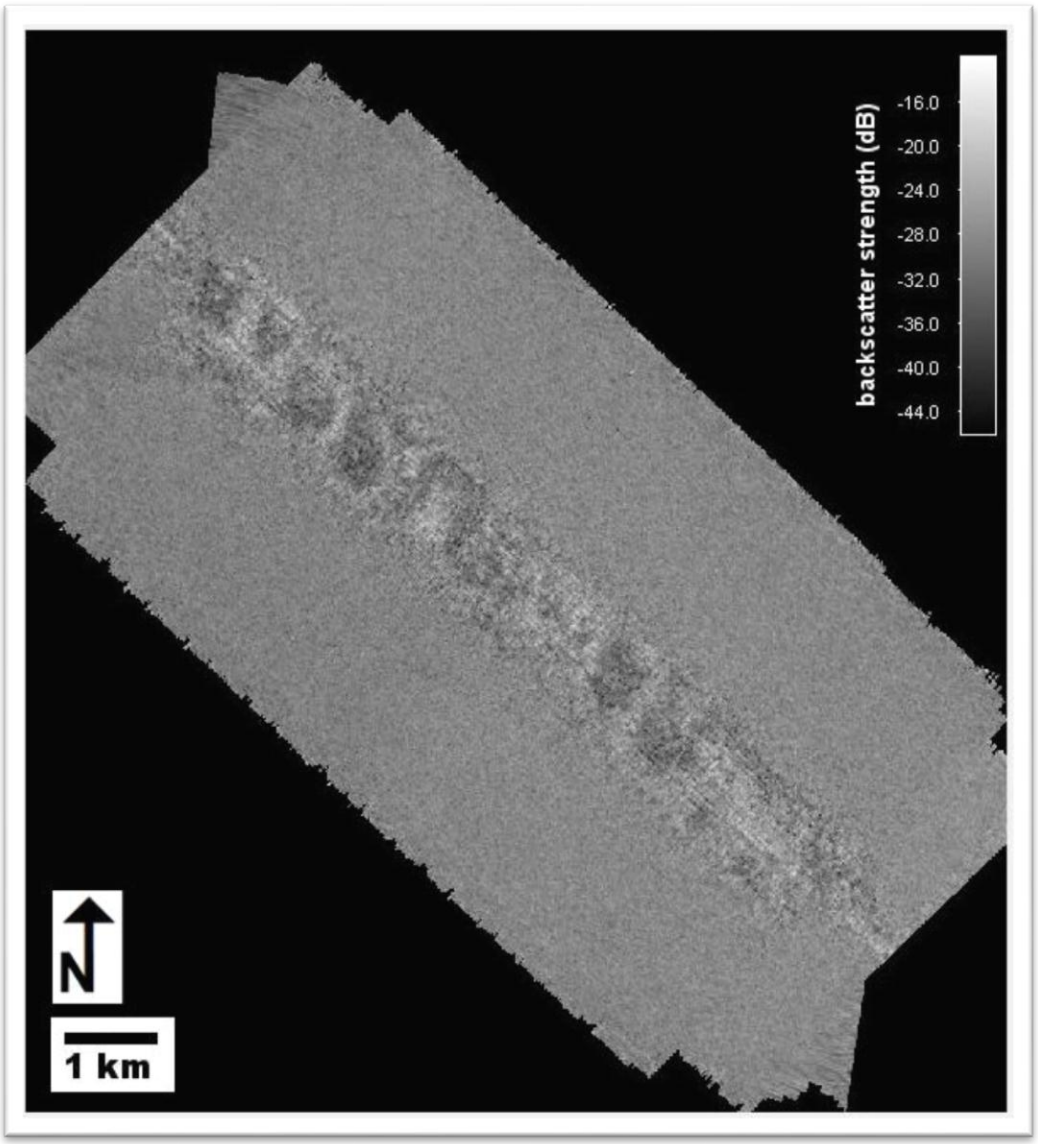

Figure 25: Backscatter mosaic (25m resolution) of the study area using multiple multibeam data.

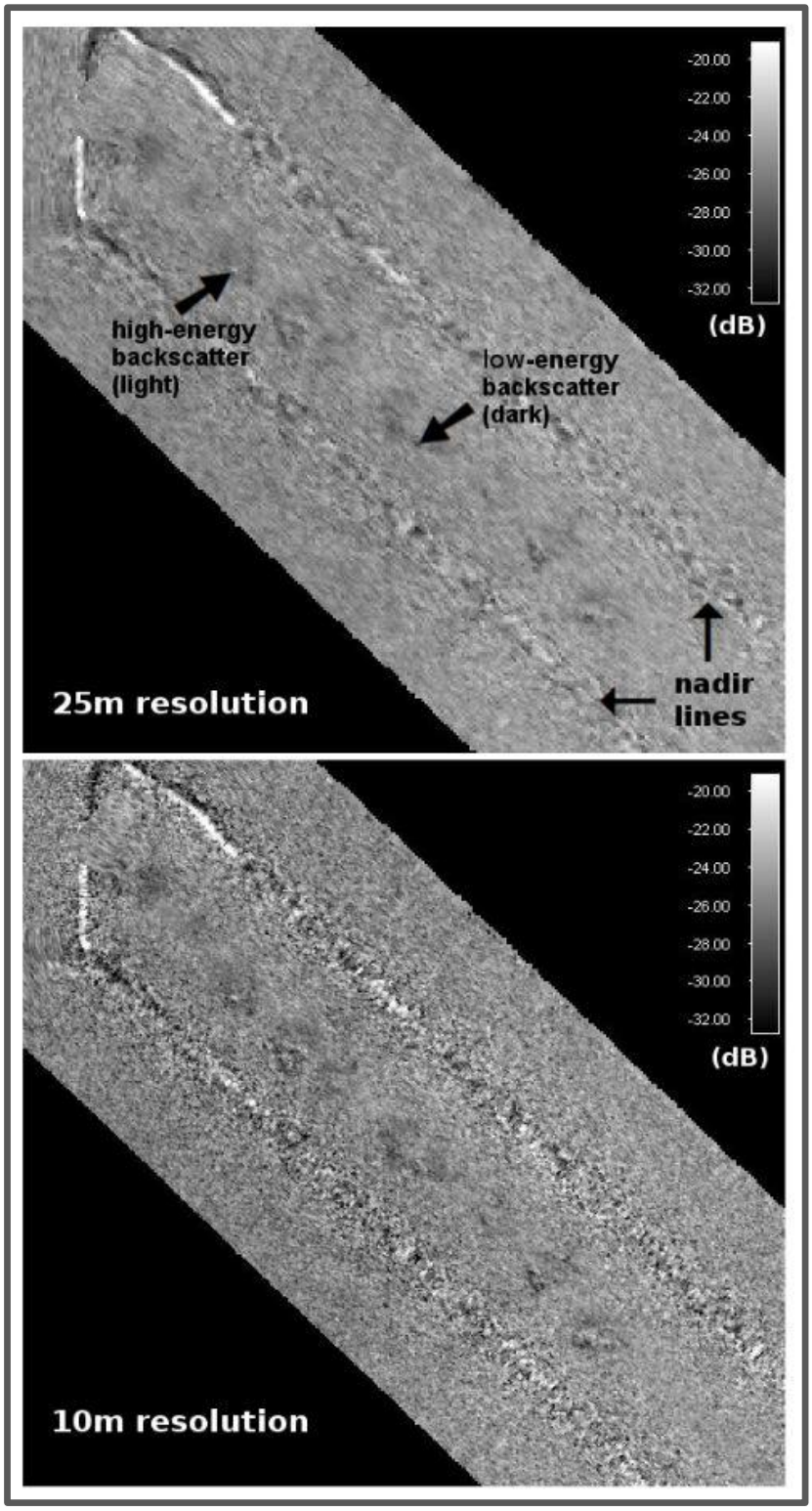

Figure 26: Backscatter mosaic using one continuous line of multibeam swaths.

4.2.2 ANGULAR RANGE ANALYSIS

Angle range analysis (ARA) can be performed to attempt to classify substrate types. This is a method of seafloor characterization which compares the actual backscatter angular response to expected acoustic response curves based on a mathematical model, in this case, the Jackson Model (Jackson et al., 1986) (Figure 27). This model generates an expected acoustic response curve as a function of grazing angle vs. returned backscatter intensity. The goal of the analysis is to attempt to characterize the measured response curve from the survey data to a best fit of a modelled curve. This modelled curve takes into account sediment properties and acoustic frequency.

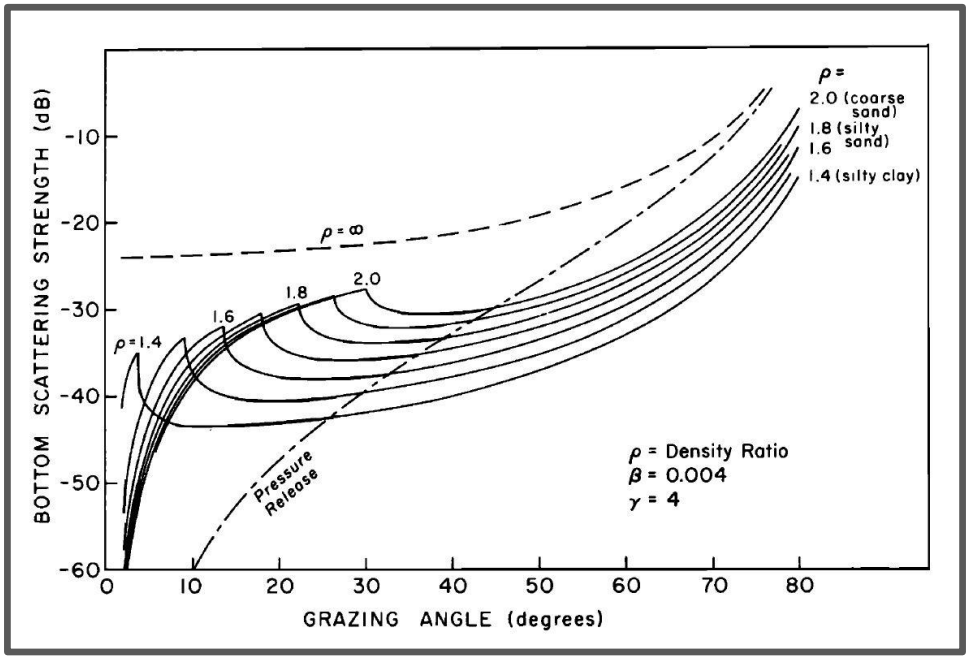

Figure 27: Jackson Model. Small-scale roughness scattering strength. (from Jackson et al., 1986)

The ARA process is relatively new so there are limitations. More ground-truthing needs to be done and the quality of the results is dependent on the system calibration and the radiometric corrections applied. The survey environment will also affect the results as ARA requires a wide coverage of grazing angles. The process does not work well in deeper water where there is often limited grazing angles. Nonetheless, the ARA process has been shown to work well for EM3002 sonars (QPS Manual, 2011), but good calibration is key.

Figure 28 shows the results of the angle range analysis to the backscatter data from the 2013 survey. The ARA map (Figure 28C) plots the predicted seabed characterization while the Patch Analyzer (Figure 28D) shows the Angle vs. Range Analysis dialog which can be viewed and edited. The default characterization is shown by the blue line but values can be manually selected for adjustments. For the 2013 survey, the resulting seabed characterization identifies clayey sand as sparsely covering the crest, muddy sand on the flanks to the east, and very fine sand covering most of the study area. This more or less agrees with a study that identifies homogeneous hemipelagic grey clay with very little amount of IRD as the upper interval of a sediment core retrieved from the western end of the Vestnesa Ridge (Consolaro et al., 2014). Another study identifies hemipelagic grey sandy mud as the upper interval from the reference core of the western Svalbard margin (Jessen et al., 2010).

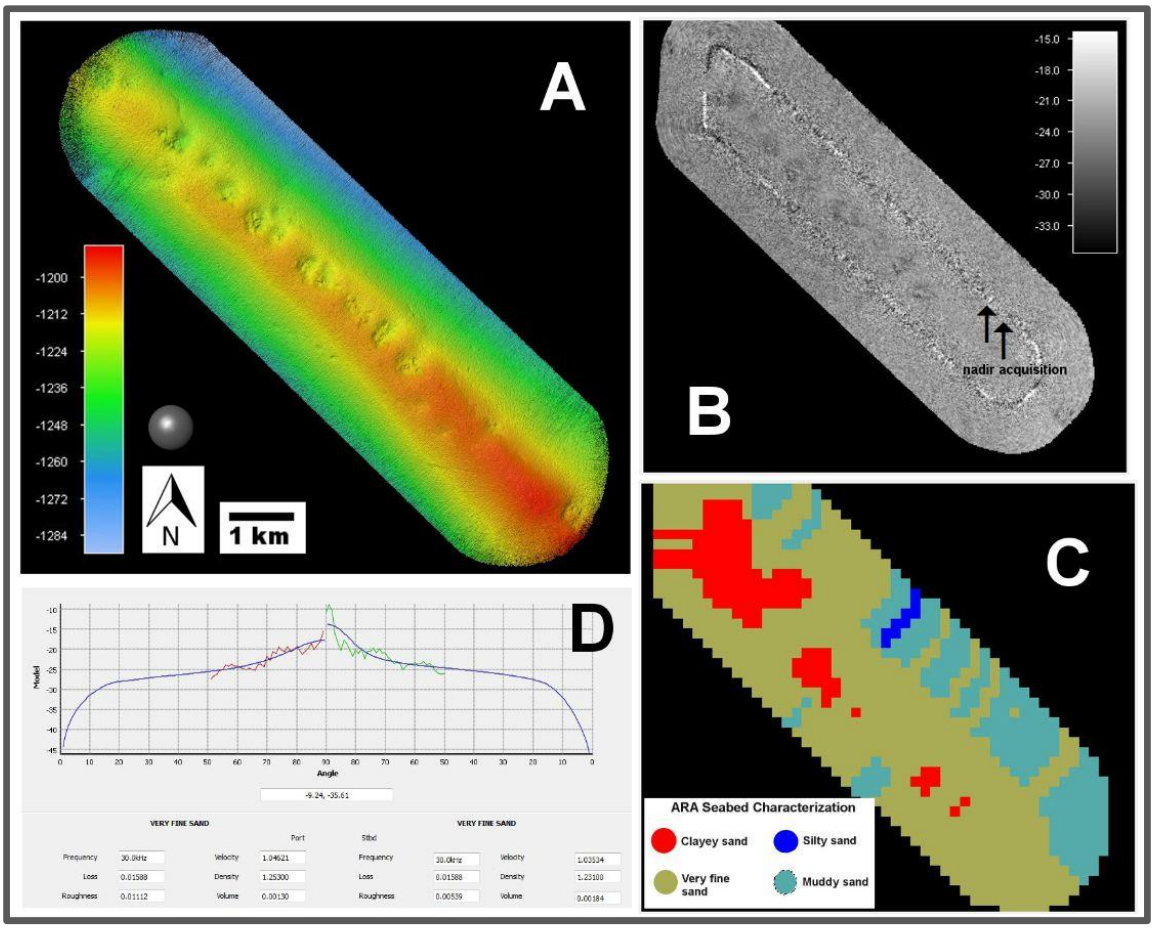

Figure 28: Angle Range Analysis (ARA) as incorporated in the Fledermaus Geocoder Toolbox. (A) Bathymetry (B) Backscatter (C) ARA analysis (D) Patch Analyzer dialog box for editing the seabed characterization parameters.

4.3 POCKMARKS

4.3.1 MORPHOLOGICAL CHANGES

A quick comparison of the profiles across two pockmarks at the southeastern part of the ridge crest show marked differences in their topographies (Figure 29). All three datasets have 10 m resolution. These same two pockmarks are among those that have been shown to be recently active due to gas flares emanating from them.

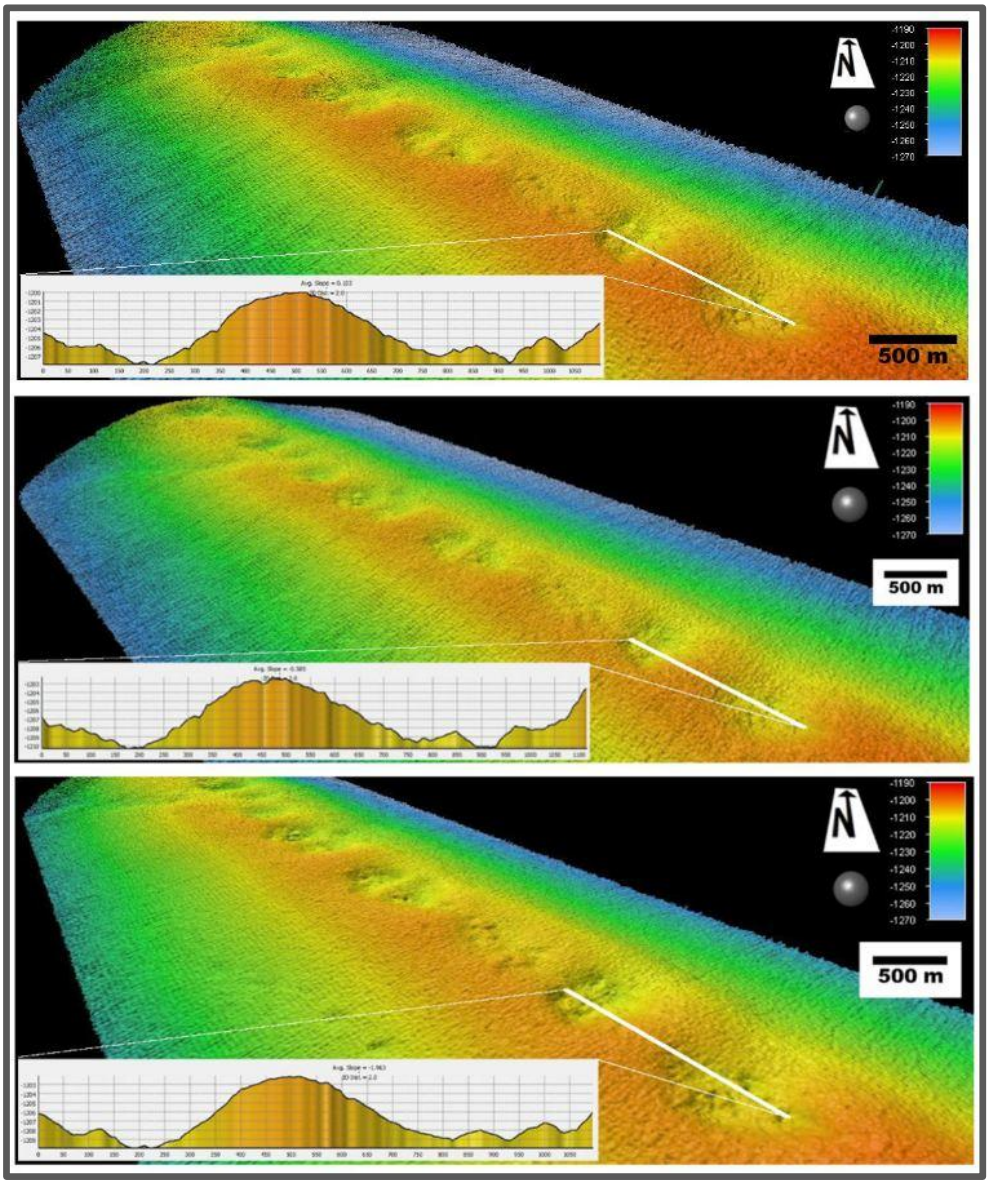

Figure 29: Profiles across the three datasets for general comparison. 2010 (top), 2012 (middle), 2013 (bottom).

As mentioned, the 2010 survey data appears to have had different re-calibration values to the multibeam echosounder system than that of the 2012 and 2013 survey data. The offset in depth is approximately 2m to as much as 3m (Figure 30). Nonetheless, surface changes can still be detected by ocular inspection of the profiles. From Figure 30, it can be seen that the pockmark to the southeast has a wider depression than in the 2010 survey. In most places along this part of the ridge, the topography is preserved whereas the pockmarks show to have more dynamic changes.

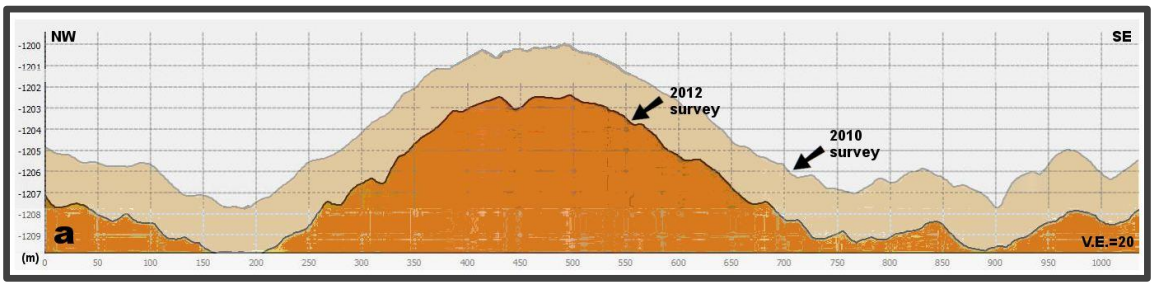

Figure 30: Profile comparison of the 2010 and 2012 datasets. The 2010 show at least 2m offset.

The pockmarks on this part of the Vestnesa Ridge generally appear circular to elliptical. They have an average long axis of 570 m and short axis of 540 m, with an average depth of 6 m. There are some pockmarks that are too close together that they seem to be forming one single pockmark. These pockmarks have especially elongated shapes with their long axes almost double their short axes. The long axis of the pockmarks seem to prefer a SW-NE orientation and their basin profiles are asymmetrical where the NE side is much lower than the SW side. This shape of the pockmarks are possibly influenced by the direction of the bottom currents.

Profiles from the 2012 and 2013 surveys are superimposed and compared along the two active pockmarks on the southeast (Figure 32). There seems to be a general increase in sediments along the ridge, of up 0.5 m on the crest. Inside the pockmarks, there appears to be both deposition and erosion. On one of the pockmarks, there is relatively little deposition. On both pockmarks there are eroded parts. These erosion surfaces could possibly be where the gas flares escape into the water column. Other examples for the leaking and non-leaking pockmarks are illustrated (Figures 33-36).

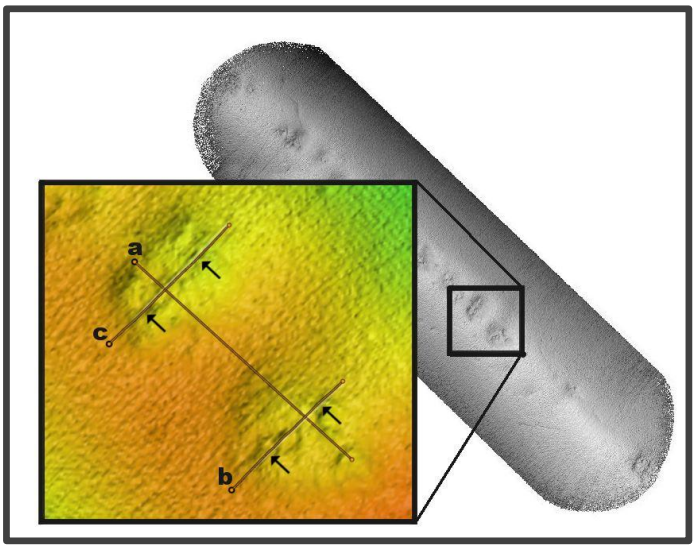

Figure 31: Location map of the 2012-2013 profiles on Figure 32.

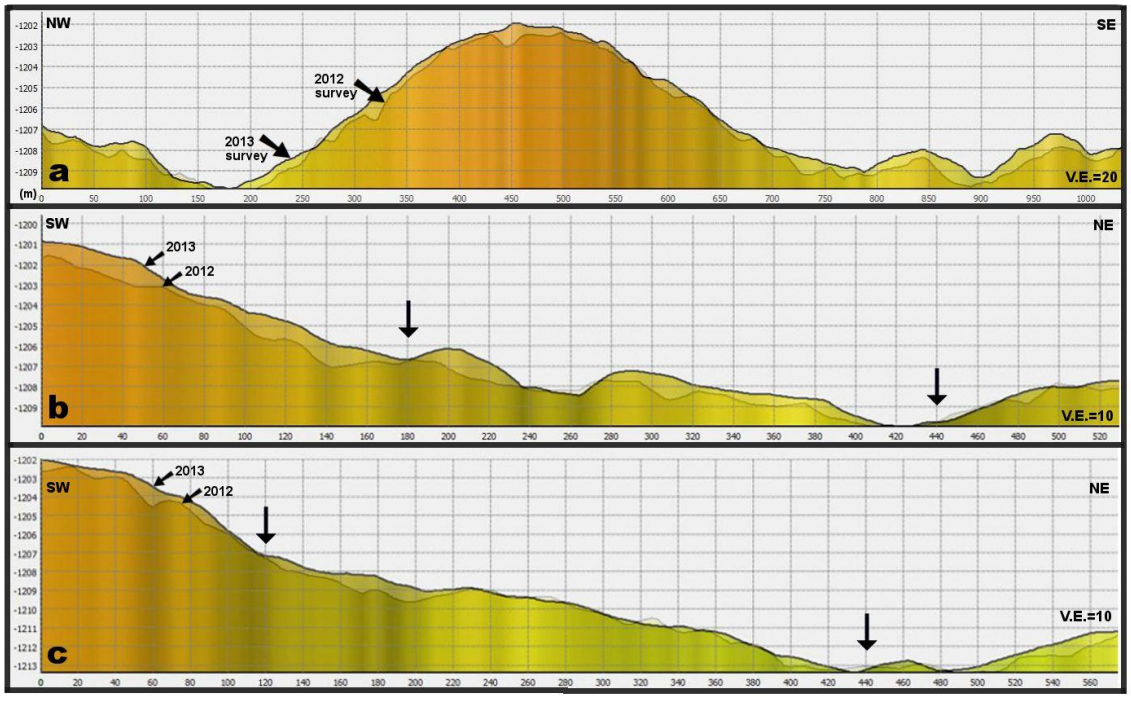

Figure 32: Profile comparison of the 2012-2013 datasets. Corresponding arrows indicate possible erosion spots.

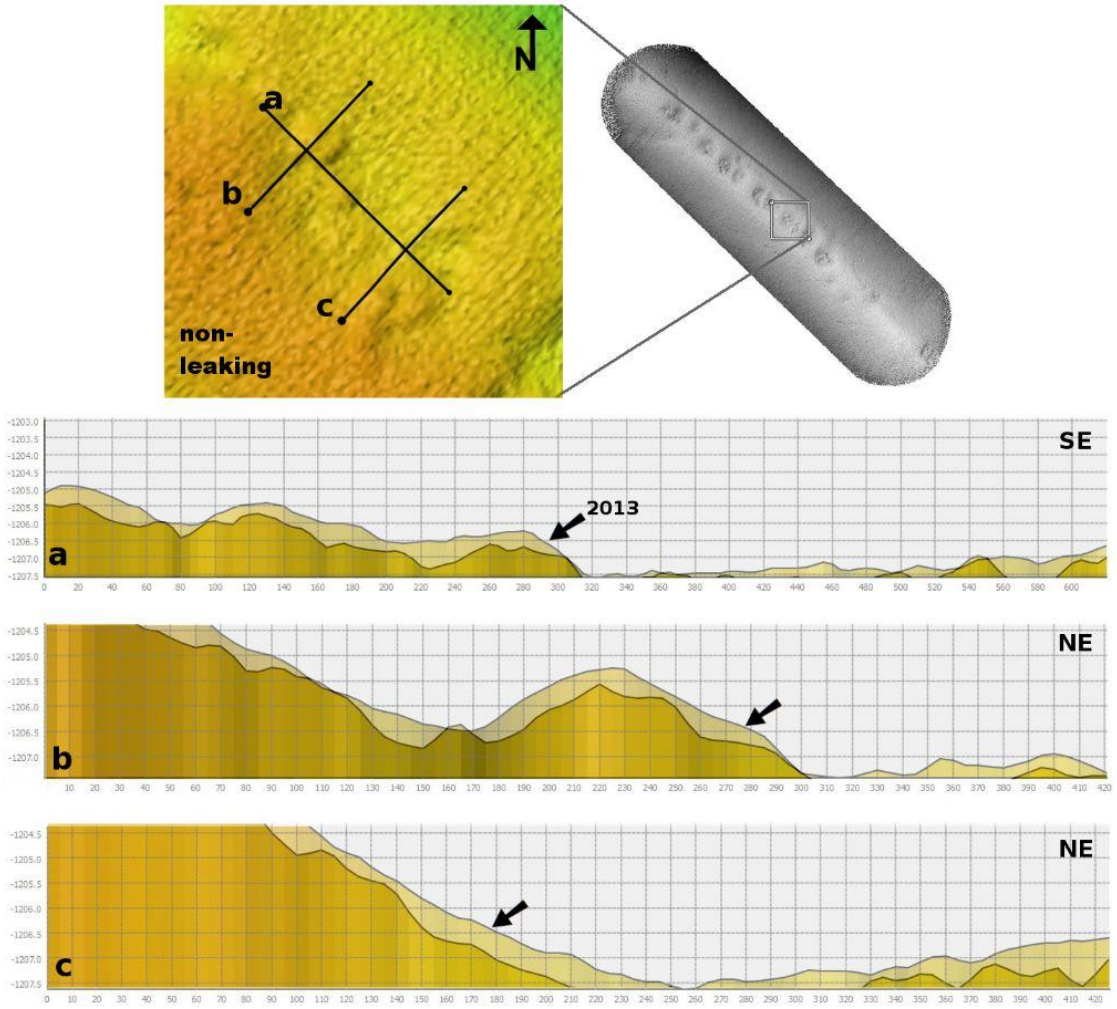

Figure 33: 2013 (indicated with arrows) and 2012 profiles across a non-leaking pockmark. The new deposits are thickest at about 0.5 m. The overlying surface appears smoother and generally follows the shape of the underlying surface, implying that this/these pockmark/s must have been inactive for a while.

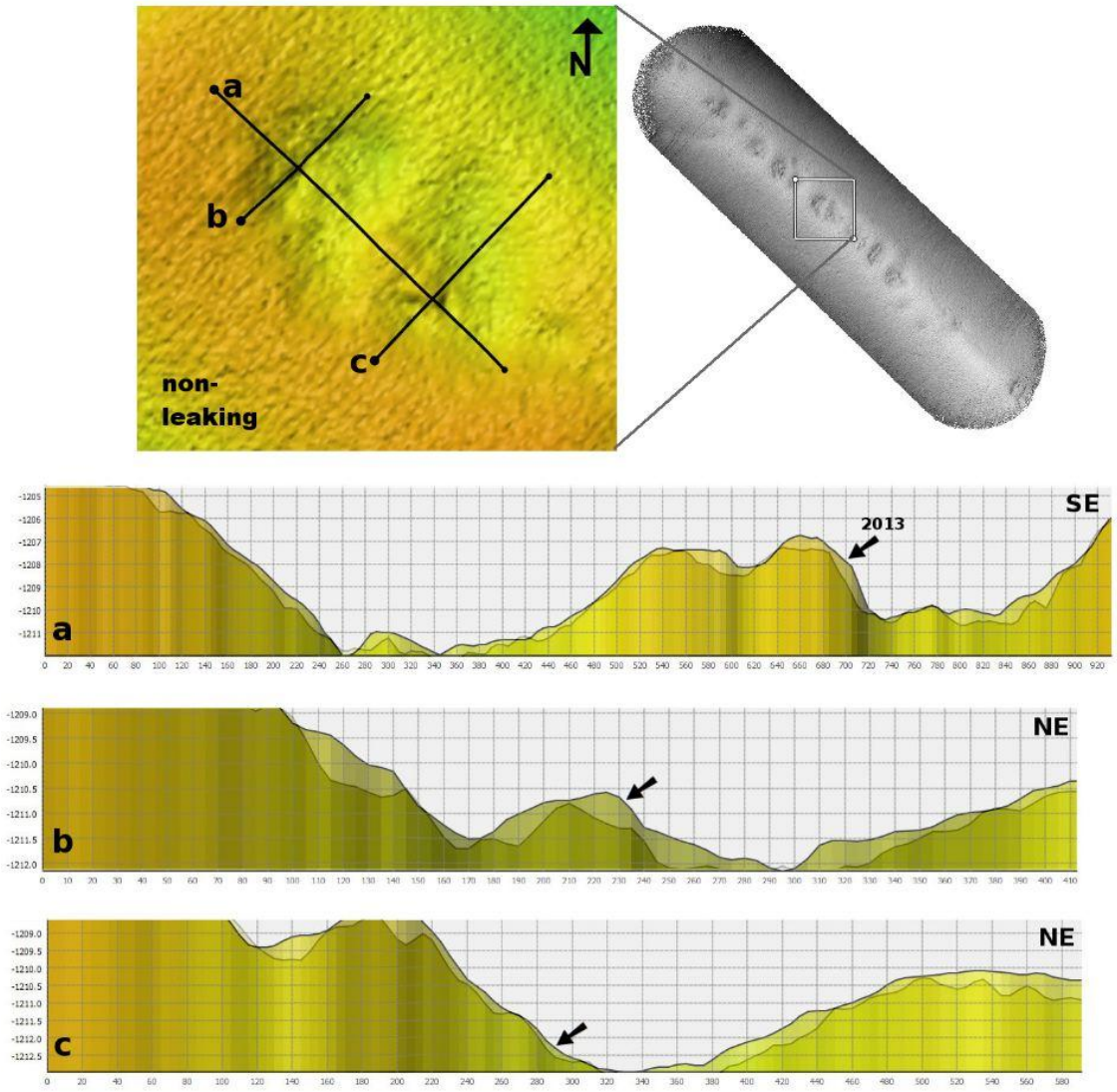

Figure 34: 2013 (indicated with arrows) and 2012 profiles across a non-leaking pockmark. This appears to be two elongated pockmarks that formed very near each other. The overlying surface also appears smoother, but the pockmarks are deep, implying that they have become inactive relatively not too long ago.

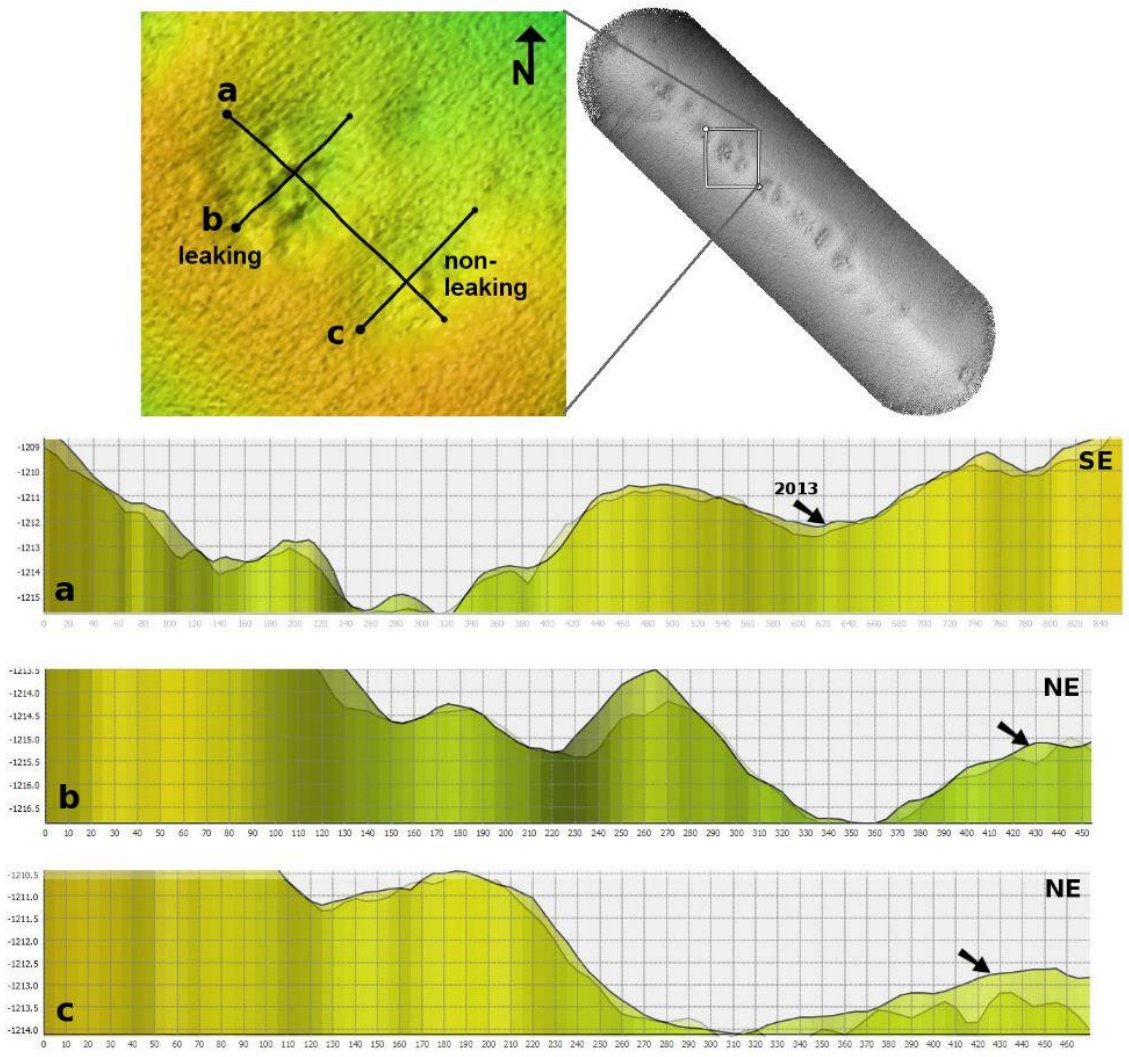

Figure 35: 2013 (indicated with arrows) and 2012 profiles across a leaking and a non-leaking pockmark. Profile (a) shows a stark contrast of the surfaces between a leaking and a non-leaking pockmark. The leaking pockmark's bathymetry is rough and deep while the inactive pockmark is smooth and shallow. Profile (b) show thicker deposition on the stoss side direction of the bottom current.

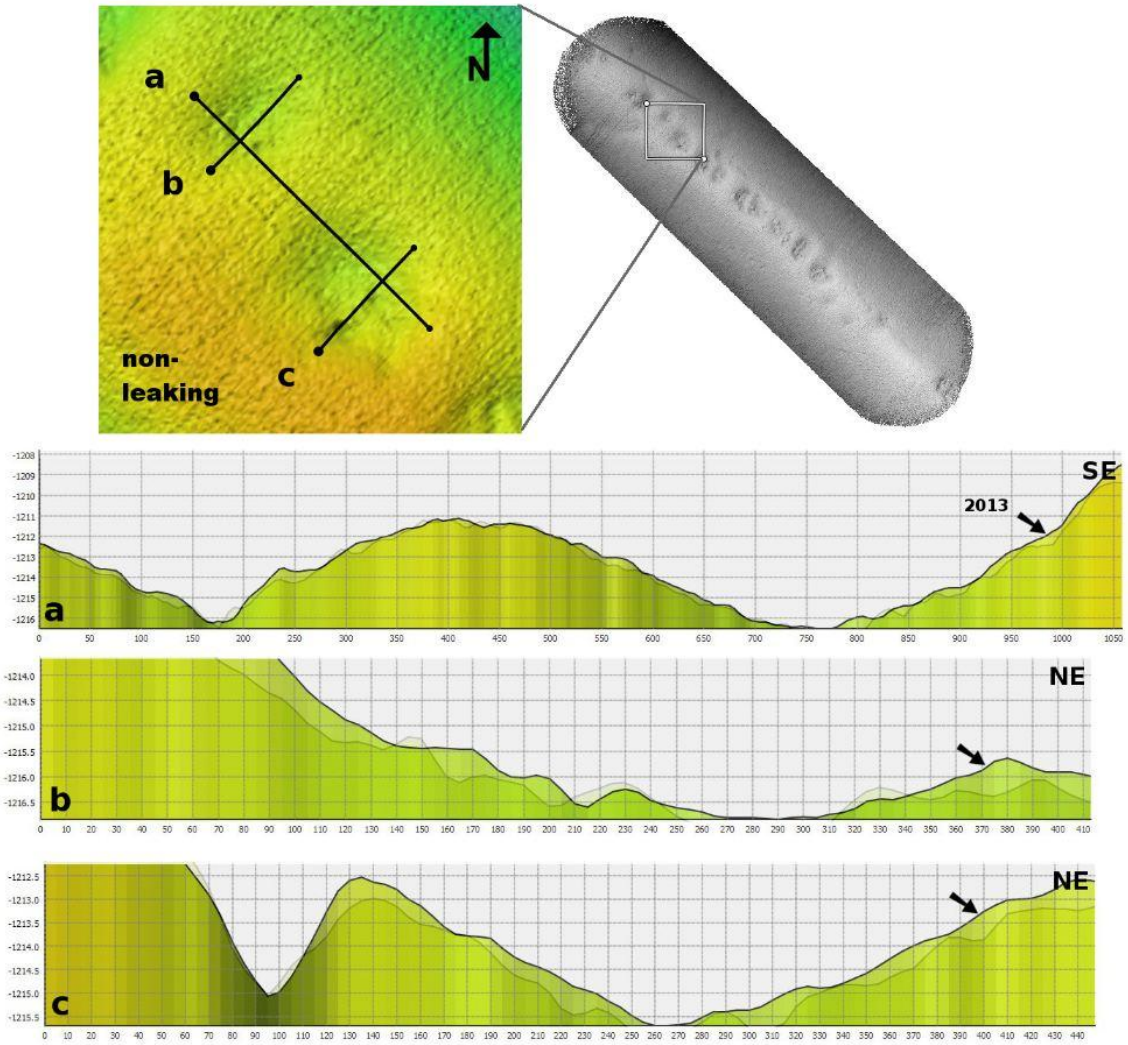

Figure 36: 2013 (indicated with arrows) and 2012 profiles across a non-leaking pockmark. These pockmarks are shallow with a funnel-like depression on Profile (c). There is no deposition on the depression and this may be due to upwelling or initial fluid activity.

4.3.2 VOLUMETRIC CHANGES

Volume change between two surfaces can be calculated from the two survey datasets with the 2012 surface data subtracted from the newer 2013 data, to record changes that has occurred in the time between the two data acquisitions. This is a good gauge of deposition within the pockmarks, especially since the bathymetric features in and around the pockmarks were double-checked and filtered, with the surfaces verified to be real features.

Figure 37 shows a simple diagram of the major pockmarks on the study area aligned NW-SE (from left to right), with the recently active ones shaded. At the bottom part of the figure are the calculated surface difference for each of these pockmarks. The dark areas are positive (deposition) and the blank areas are negative (erosion). The software-calculated net deposition inside the pockmarks ranges from 5 288 m^3 to 62 277 m^3. Active pockmarks pm2, pm3, pm6 and pm9 also show net deposition, but on their edges towards SW, there are blank patches. It is possible that gas escapes on these areas of non-deposition.

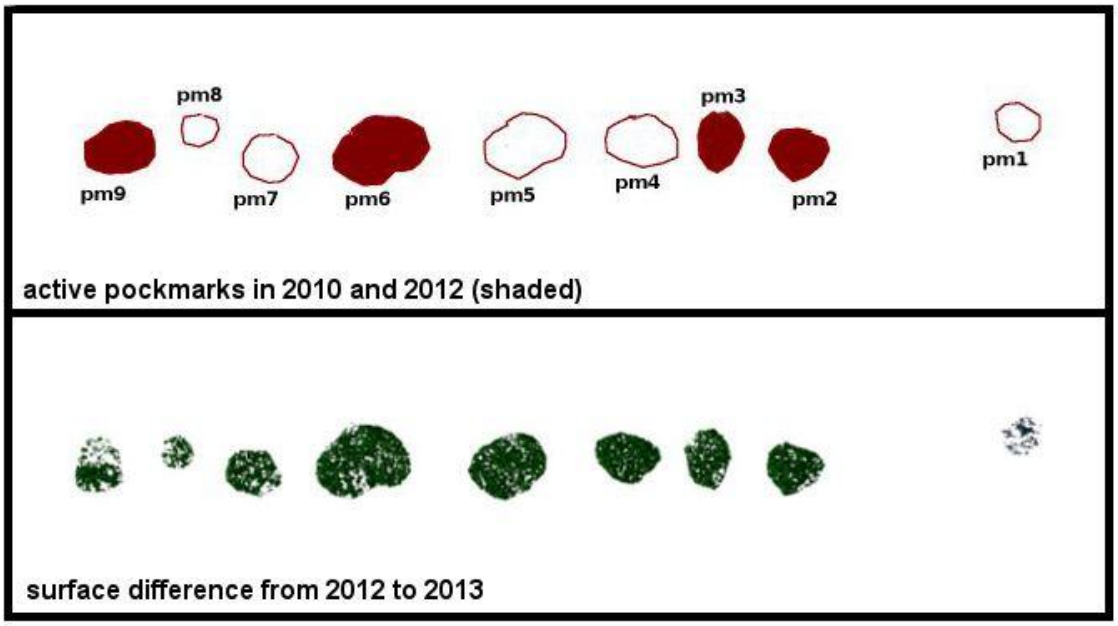

Figure 37: Upper: Diagram of pockmarks along the ridge crest oriented NW-SE (left to right). The pockmarks with observed recent activity are shaded red. Lower: Surface difference plots between the 2012 and the 2013 surfaces. The plot represents positive difference that indicates net deposition.

A combination of different types of data (bathymetry, profile, backscatter, surface difference, gas flares) suggest that activity within these pockmarks are localized to a specific area. The eroded surface on the bathymetry profile, the low intensity backscatter, the negative patches on the surface difference plot, seem to agree with earlier observations that gas seeps originate from the SW edge of these two pockmarks (shaded area on Figure 38D). This corresponds to earlier observations and studies on the gas flares emanating from these pockmarks (Figure 38 inset).

The surface difference plot (Figure 38C) also show negative values to the NE of the pockmarks, suggesting erosional processes going in that direction, down the ridge flank and further down into the adjacent trough.

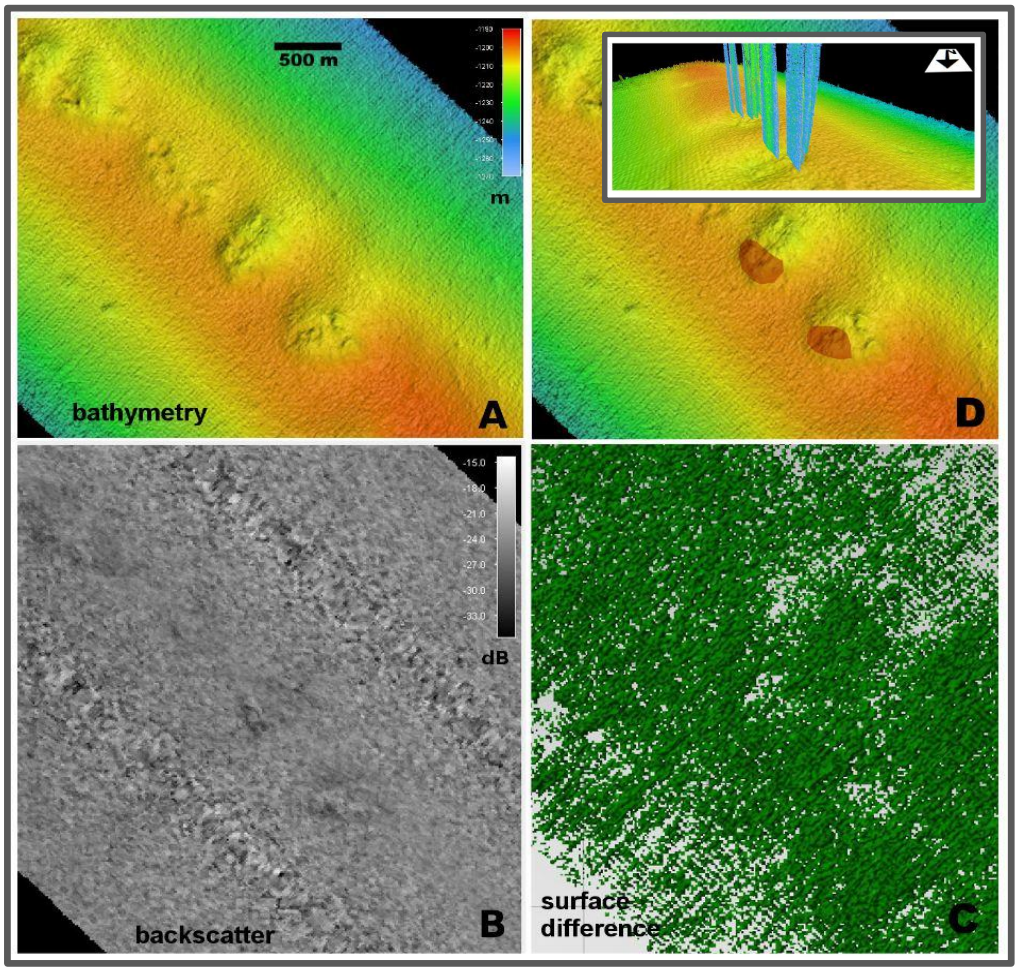

Figure 38: Different representations of the seafloor with the two active pockmarks. (A) Bathymetry showing the inner structure of the pockmarks. (B) Backscatter showing low-intensity dark patches on the SW half of the pockmarks. (C) Surface difference (2013-2012) plot showing non-deposition on the SW half of the pockmarks. (D) Interpreted source of gas flares from inside the pockmarks, which corresponds to the plotted source of gas flares (D inset) observed in earlier studies by Bünz et al., 2012 and Smith et al., 2014.

4.4 POCKMARK FIELD NORTH OF THE STUDY AREA

Backscatter data remains a very useful tool in detecting features on the seafloor that are not discernible on bathymetry data. In this example from a pockmark field in the northwestern part of the Vestnesa Ridge (Figure 39), high backscatter is detected on the pockmarks that are randomly distributed on the seafloor, suggesting the presence of carbonates or hydrates. On the other side of the bend, the evenly distributed pockmarks along the crest of the ridge to the east are only faintly detected as grey low-energy backscatter. This could point to different mechanisms of fluid flow and gas release between these two distinct pockmark fields.

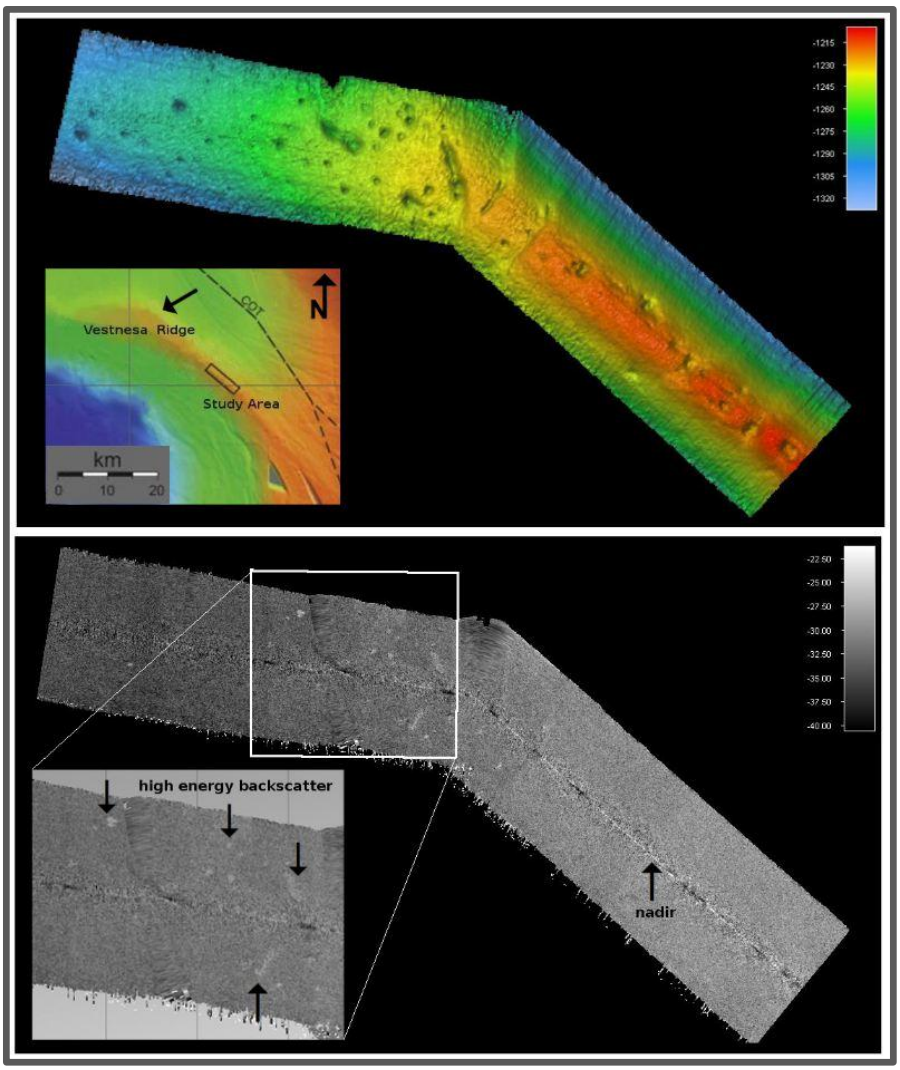

Figure 39: Bathymetry and backscatter of a pockmark field in the northwestern end of the Vestnesa Ridge. The arrow on the inset points to the location of the swath. High backscatter on the unevenly distributed pockmarks to the NW are distinguishable while linear bigger pockmarks to the SE show as faint low-energy backscatter

5 DISCUSSION

5.1 Pockmark morphology

Elongate shape

Pockmarks are circular to elongated depressions on the seafloor, commonly occurring especially on the continental shelf throughout the world (Hovland and Judd, 1988, Hovland et al., 2002). Elongated pockmarks commonly occur in areas influenced by strong bottom currents capable of eroding the newly formed pockmarks (Hovland et al., 2002). These elongated pockmarks are often aligned along prevailing current directions, which may indicate that the pockmarks were initially circular, but have been deformed by sediment transport, deposition, and erosion (Josenhans et al., 1978; Hovland, 1983; Bøe et al., 1998). Furthermore, erosion by bottom current will be most significant on the downstream side of the pockmark, resulting in an asymmetrical shape where they develop deepest upstream (Josenhans et al., 1978).

The pockmarks on southeastern part of the ridge are mostly elongated, with the long axis oriented SW-NE. They have asymmetrical profiles (Figure 32) with the steeper part upstream. The surface difference of the 2013 and 2012 bathymetry show negative values where the erosion of the bottom currents is supposed to have occurred. While other processes such as creeping, or other down-slope processes may also occur, it is highly likely that very strong bottom currents exist at the crest of the Vestnesa Ridge that are capable of eroding or shaping these pockmarks.

Presence or lack of infill

Coarse sediment is often found in the center of pockmarks. In some cases, this is due to authigenic carbonate in methane seep settings, or may be explained as a winnowed lag deposit caused by the expulsion or seepage of fluids. Such lag deposits can also be due to currents, as well as to the accumulation of other debris (Hovland et al., 2002). Bathymetric data show that there has been deposition in the pockmarks with both low and medium backscatter values, with homogenous fine sediments (low backscatter) and coarser sediments (medium) as assumed infill. In general, pockmarks that inactive have a smoother morphology than those documented to be leaking (Figure 40),

In some places, the pockmarks appear to have no deposition, and with net erosion. Hammer et al. (2009) suggested that currents may be deflected by the pockmark in a way that produces a positive vertical current component from the pockmark. This upwelling phenomenon could lead to reduced sedimentation rate, and winnowing of inside the pockmark. This upwelling is an effect of deflected currents, not of expulsion of fluids or gas from the seafloor, and is sufficiently strong to prevent the settling of fine particles. This reduction in sedimentation rate over the pockmarks (relative to that of the flat surrounding seabed) explain the lack of infill in pockmarks even when it is inactive. The lower relative sedimentation rate inside the pockmark could even make it deepen over time, as was the case in the bathymetric changes in this dataset.

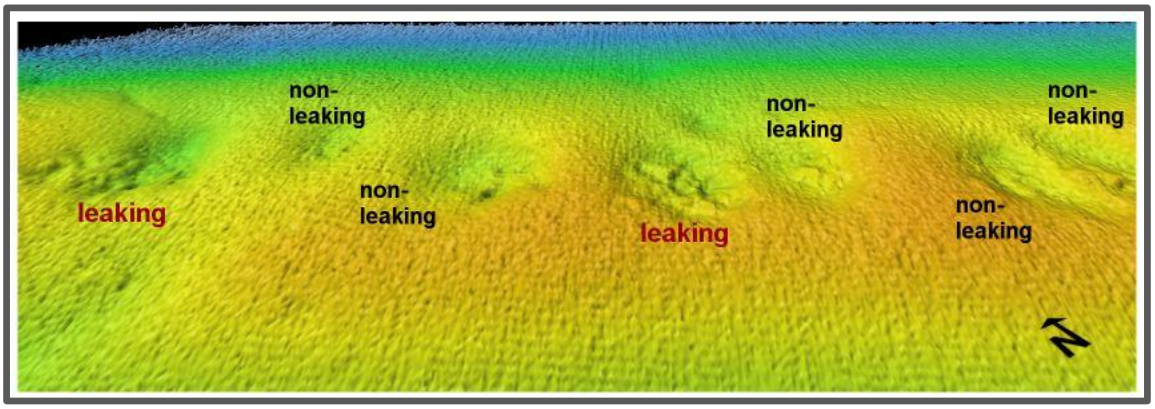

Figure 40: 10 m resolution bathymetry of a portion of the Vestnesa Ridge. Leaking pockmarks have a more uneven morphology, while non-leaking pockmarks are smoother.

Advancing pockmark

A study by Ho et al. (2012) looked into advancing pockmark arrays as a record of paleo-fluid processes. Buried channels or deep faults provide conduits for fluid flow, with degassing most likely occurring along the axis of the buried channel during times of lower sea level. The lateral advancement of pockmarks subsequently results from the interplay between fluid venting and generation of local depressions in the sediment surface, and the perturbation of bottom currents within the depression. For the advancing pockmark location, fluid flow variations control the creation of pre-existing topography, which in turn controls the location of sedimentary accumulation. The lateral migration of the pockmark terminates when fluid venting ceases. Once fluid venting stops, new depressions cease to form and are buried by subsequent sedimentation (Figure 41).

While this model does not adequately account for the fluid migration on the ridge crest, this can explain the truncation of sediments in the pockmarks on the downstream side towards the NE.

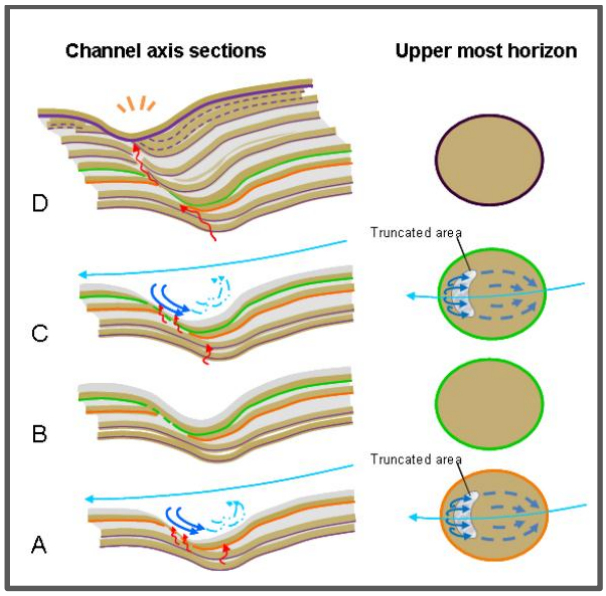

Figure 41: Model for the development of advancing pockmarks. (A) Fine-grained sand on the downstream pockmarks sidewall re-suspended by vortex and seepage. A horseshoe-shaped truncated area was formed. (B) The infill phase may occur during times of reduced bottom-water current activity. Thus horseshoe-shaped void was filled by the new deposits. (C) Stage A repeated after a new layer deposited. (D) Lateral migration by the creation of secondary pockmarks, which truncated the downslope flank of the preceding infill sequence. (from Ho et al., 2012)

5.2 Backscatter data

Backscatter interpretation

Pockmarks on Vestnesa Ridge are characterized by both high and low backscatter intensity relative to the surrounding seafloor. The high amplitudes may be indicative for precipitated carbonate and/or hydrate formation at or near the seafloor whereas low reflectivity reflects soft, muddy sediment probably being altered by fluid expulsion (Petersen and Buenz, 2008).

The backscatter data of the study area (Figure 26) show more or less a homogenous composition on the flanks of the ridge. The crest is interspersed with low backscatter areas corresponding to the pockmarks, with medium-high backscatter inside and around the pockmarks. The low backscatter value inside the pockmarks could be interpreted as an angle of incidence effect, with the surface facing away from the beam. The SW half of the pockmarks generally appear darker than the other half, and this could be due to the steepness and depth of the upstream side of the ridge, while the downstream side slopes more gently and so has relatively higher backscatter. The backscatter contrast could also be due to sediment-property differences between the sediments covering the pockmark, e.g. differences in grain size distribution induced by prevailing currents (Todd, 2005). This scenario is possible since the 2013 data shows net erosion on the part of the pockmarks that have low backscatter. Inside some pockmarks, there appears to be material or sediments in the middle that has higher backscatter. This can possibly be course sediments or debris reworked by currents, as backscatter is influenced by the physical characteristics of the surface, that is, rougher surfaces have higher backscatter. The presence of bubbles in the sediments or close to the seafloor can also contribute to higher backscatter at this water depth (Fonseca et al., 2002).

A more likely explanation for the relatively high backscatter material inside the pockmarks on the crest is that it indicates carbonate or hydrate presence. Seabed cold seeps may be recognized by distinctive morphological and/or backscatter signatures on sonar images. Authigenic carbonates are known to be major contributors to seafloor roughness and acoustic impedance contrast in cold seep areas, and thus also to acoustic backscatter intensity (Johnson et al., 2003). In particular, a strong difference in impedance contrast, small-scale roughness and morphology between carbonate precipitates and the seafloor produces elevated backscatter in sonar images from which seep carbonates can be identified (Johnson et al., 2003; Holland et al., 2006). This is especially true for marine environments with muddy, hemipelagic seafloor sediments that are of low backscatter.

In a study by Naudts et al. (2008) of the backscatter patterns in a methane venting area, it was observed that methane seeps are in areas with medium- to high-backscatter strength, and not in areas with very high and maximum backscatter strength. They explained that the absence of active seeps in areas with the highest backscatter values supports the model proposed by Hovland (2002), in which AOM-induced carbonate formation may lead to self-sealing of fluid pathways by carbonate clogging, followed by a relocation of the fluid/gas pathways around the cemented, impermeable areas. They concluded that the observed backscatter patterns are the result of ongoing methane seepage and the precipitation of MDACs (methane-derived authigenic carbonates) caused by AOM (anaerobic oxidation of methane), and the carbonate formation also appears to lead to a gradual (self)-sealing of the seeps by cementing fluid pathways/horizons followed by a relocation of the bubble-releasing locations (Naudts et al., 2008).

The Vestnesa Ridge has methane seeps and is also found to have methane-derived carbonates and gas hydrates from gravity and piston cores retrieved from the around the pockmarks of the study area (Smith et al., 2014). It is therefore possible that this part of the ridge exhibits the gradual self-sealing of the seeps, albeit in lesser extent since there have not been observed high backscatter (massive carbonate precipitates)

in the study area, rather, medium backscatter values in and around the pockmarks (Figure 42). The medium backscatter is nonetheless characteristic of areas with methane seeps. This slightly elevated backscatter have been attributed by Klaucke et al. (2010) to the presence of gas bubbles or even gas hydrate in the shallow subsurface, both of which is the case in this area of the Vestnesa Ridge. It can be also be that methane-derived carbonates acts as seal on the surface or the shallow subsurface, and could likely explain the varied backscatter response from the different pockmarks on the crest, and ultimately, why some of the pockmarks or some parts of the pockmarks are inactive. A clearer relationship between inactive (assumed to be sealed with carbonate precipitates) pockmarks on this area and the backscatter response can most likely be determined from a better quality backscatter data.

The pockmark field north of the study area (Figure 39) can be interpreted thus as having methane-derived carbonate precipitates from the high backscatter observed on some of the pockmarks. It is likely that the areas with high backscatter are sealed and no methane release is occurring where the carbonate seals are.

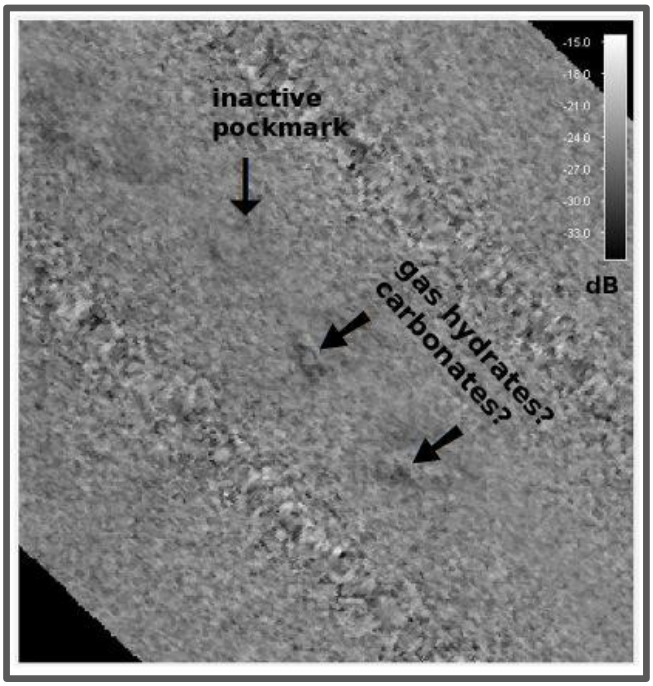

Figure 42: Backscatter of pockmarks that possibly containing gas hydrates or carbonate precipitates. The active pockmarks show a high contrast in backscatter value while the inactive pockmark is hardly discernible.

Backscatter data quality

The backscatter was processed at 25 m resolution, the best possible for the acquired data. The backscatter data was acquired by the same installation as the EM300 multibeam echosounder. Multibeam systems, however, are optimized for bottom detection and not backscatter sampling. Small amounts of noise that have negligible effect on bathymetry data quality may have a big effect on the backscatter data. For example, a 200 kHz multibeam can be operated simultaneously with a 100 kHz single beam echosounder without any measurable interference in the bathymetric data; but the interference pattern from the single beam will be clearly visible in the backscatter record (Blondel, 2009).

During the surveys, single-beam echosounder data were also acquired using a Simrad EK60 system operating at frequencies of 18, 38 and 120 kHz to detect gas bubbles in the water column. The interference from the single beam acquisition has likely compromised the backscatter record of the EM300 multibeam for the study area. In areas where there were no apparent interference, such as the pockmark field further north where the ridge bends (Figure 39), the backscatter record was less noisy and the resolution is higher at 11 m. In any case, backscatter record from multibeam systems is sufficient and even has proven to work well with ARA analysis of seabed characterization (Fonseca and Calder, 2005), provided there are no interference and/or operating at high frequencies.

5.3 Fluid flow controls

Faults

The Vestnesa Ridge sits on young oceanic crust where the eastern part is approximately 20 My and the western part is less than 10 My. The western end of the ridge is about 40 km away from the Molloy Ridge. Shallow crustal seismicity associated with the mid-ocean spreading triggers active faulting in the region.

Extensional faulting plays a key role in the supply and distribution of methane hydrate and free gas across the Vestnesa Ridge (Hustoft et al., 2009). This extensional faulting is a continuous process related to the nearby rifting and/or thermal subsidence of the young basin. Hustoft et al. (2009) interpreted several faults beneath the Vestnesa Ridge, to a depth extent down to the YP1 unit, which lies at ~-3500 ms (TWT) beneath this part of the ridge. These faults are related to the nearby Knipovich Ridge and the Molloy Transform Fault Zone and has an SE orientation, approximately strike-parallel to the COT that runs SE– NW. The same study also found that peak saturations of both gas hydrate and free gas occurring at the crest of the ridge and in immediate vicinity of extensional faults, implying a strong relationship between the faults and fluid flow in the ridge.

The apparent activity within the pockmarks as observed in this study, where it is assumed that only the SW half of at least 4 of the pockmarks are leaking, can be related to the location of the SE oriented fault within the pockmark-chimney system. It is possible that the upward migration of gas/fluids is strongly fault-controlled and the free pathway for the gases or pore fluids is through a common fault that cuts through the ridge. This can explain the preference of the gas leaks to the SW part of the pockmarks.

Carbonate/Hydrate seal

The pockmarks on the crest of Vestnesa Ridge are connected to acoustically transparent zones in the sediment that extend from the seabed to depths below the BSR. These conduits are interpreted as gas chimneys where free gas is migrating through the HSZ (Bünz et al., 2012). Seismic data suggest that these chimneys are fed by a critically pressured free-gas column beneath the BSR (Hustoft et al., 2009; Bünz et al., 2012). The heterogeneous distribution of high-amplitude reflections above the BSR and at shallower depth suggests formation of massive hydrate and/or authigenic carbonate in the vicinity of multi-fractured fluid pathways (Petersen). Geochemical analyses by Smith et al has shown that a thermogenic source is supplying methane and other light hydrocarbons to the ridge, and piston and gravity cores recovered gas hydrate and carbonates (Smith et al., 2014).

Fluid migration can be influenced by carbonate precipitation (Hovland et al., 2002) and the build-up of an internal reservoir (Leifer et al., 2004). Carbonate precipitation that over time cements the migration pathways, gradually reducing fluid escape and leading to self-sealing of seeps (Hovland et al., 2002). In other cases, the fluid flow is controlled by a capacitor, which is described as a reservoir that has to fill up first before conditions for fluid release are met, gas hydrates acting as such capacitor (Klaucke et al., 2010).

Backscatter data has shown a possible gas hydrate or carbonate precipitate inside the pockmarks in the study area. Although the backscatter values are not very high, there is apparent contrast in backscatter inside the pockmarks. Information from other studies (presence of carbonate and gas hydrate in the subsurface, active methane gas leaks, fluid migration through faults, gas chimneys, inactive pockmarks), combined with the backscatter data and some of the observations in this paper (apparent preferred leak location in the pockmarks, influence of bottom currents on the pockmarks) point to a mechanism where carbonate formation leads to self-sealing, followed by relocation of the fluid pathways, or eventual inactivity.

6 CONCLUSION

- The pockmarks on the crest of the southeastern part of the Vestnesa Ridge show a preferred SW-NE orientation.

- The pockmarks have asymmetrical profiles with the steeper part upstream and erosion on the downstream part.

- The orientation and shape of the pockmarks is controlled by bottom currents of the West Spitsbergen Current flowing northeast above the ridge.

- Upwelling is likely causing a relatively low deposition rate on the pockmarks.

- Continuous gas release from the active pockmarks is apparent when the bathymetric surfaces from 2012 to 2013 were compared. The section of the pockmarks where the gas flares originate show no net deposition.

- Backscatter data show a medium backscatter value material, possibly gas hydrate or carbonate precipitate, inside the pockmarks.

- Backscatter recording without interference from simultaneous bottom surveys yield a higher resolution data.

- Gas leaks has a preferred location of release on the pockmarks that could relate to the orientation of faults on the ridge.

- The inactivity in some pockmarks or in some parts of the pockmarks is possibly caused by carbonate or hydrate clogging on the surface or the subsurface.

References

Aagaard, K., A. Foldvik and S. R. Hillman (1987). "The West Spitsbergen Current: Disposition and Water Mass Transformation." J. Geophys. Res. **92**(C4): 3778-3784.

Aagaard, K., J. H. Swift and E. C. Carmack (1985). "Thermohaline Circulation in the Arctic Mediterranean Seas." J. Geophys. Res. **90**(C3): 4833-4846.

Aksenov, Y., S. Bacon, A. C. Coward and A. J. G. Nurser (2010). "The North Atlantic inflow to the Arctic Ocean: High-resolution model study." Journal of Marine Systems **79**(1-2): 1-22.

Andersen, E. S., T. M. Dokken, A. Elverhøi, A. Solheim and I. Fossen (1996). "Late quaternary sedimentation and glacial history of the western Svalbard continental margin." Marine Geology **133**(3-4): 123-156.

Anderson, A. L. and L. D. Hampton (1980). "Acoustics of gas-bearing sediments I. Background." The Journal of the Acoustical Society of America **67**(6): 1865-1889.

Andreassen, K., P. E. Hart and A. Grantz (1995). "Seismic studies of a bottom simulating reflection related to gas hydrate beneath the continental margin of the Beaufort Sea." J. Geophys. Res. **100**(B7): 12659-12673.

Andreassen, K., E. Nilssen and C. Ødegaard (2007). "Analysis of shallow gas and fluid migration within the Plio-Pleistocene sedimentary succession of the SW Barents Sea continental margin using 3D seismic data." Geo-Marine Letters **27**(2): 155-171.

Blondel, P. (2009). The handbook of sidescan sonar, Springer.

Bünz, S. and J. Mienert (2004). "Acoustic imaging of gas hydrate and free gas at the Storegga Slide." J. Geophys. Res. **109**(B4): B04102.

Bünz, S., S. Polyanov, S. Vadakkepuliyambatta, C. Consolaro and J. Mienert (2012). "Active gas venting through hydrate-bearing sediments on the Vestnesa Ridge, offshore W-Svalbard." Marine Geology **332–334**(0): 189-197.

Bøe, R., L. Rise and D. Ottesen (1998). "Elongate depressions on the southern slope of the Norwegian Trench (Skagerrak): morphology and evolution." Marine Geology **146**(1): 191-203.

Cokelet, E. D., N. Tervalon and J. G. Bellingham (2008). "Hydrography of the West Spitsbergen Current, Svalbard Branch: Autumn 2001." J. Geophys. Res. **113**(C1): C01006.

Consolaro, C., T. Rasmussen, G. Panieri, J. Mienert, S. Bünz and K. Sztybor (2014). "Carbon isotope (δ 13 C) excursions suggest times of major methane release during the last 14 ka in Fram Strait, the deep-water gateway to the Arctic." Carbon **10**: 4191-4227.

Demenitskaya, R. M. and A. M. Karasik (1969). "The active rift system of the Arctic Ocean." Tectonophysics **8**(4-6): 345-351.

Dillon, W. P. and C. K. Paull (1983). "Marine gas- hydrates: II. Geophysical evidence, Cox, J. L. (ed Natural Gas Hydrates: properties, occurrence and Recovery)." 73-90.

Eiken, O. and K. Hinz (1993). "Contourites in the Fram Strait." Sedimentary Geology **82**(1-4): 15-32.

Eldholm, O., J. I. Faleide and A. M. Myhre (1987). "Continent-ocean transition at the western Barents Sea/Svalbard continental margin." Geology **15**(12): 1118-1122.

Fahrbach, E., J. Meincke, S. Østerhus, G. Rohardt, U. Schauer, V. Tverberg and J. Verduin (2001). "Direct measurements of volume transports through Fram Strait." Polar Research **20**(2): 217-224.

Faleide, J. I., S. T. Gudlaugsson, O. Eldholm, A. M. Myhre and H. R. Jackson (1991). "Deep seismic transects across the sheared western Barents Sea-Svalbard continental margin." Tectonophysics **189**(1-4): 73-89.

Faugères, J. C., M. L. Mézerais and D. A. V. Stow (1993). "Contourite drift types and their distribution in the North and South Atlantic Ocean basins." Sedimentary Geology **82**(1-4): 189-203.

Fonseca, L. and B. Calder (2005). Geocoder: an efficient backscatter map constructor. Proceedings of the US Hydrographic Conference.

Fonseca, L., L. Mayer, D. Orange and N. Driscoll (2002). "The high-frequency backscattering angular response of gassy sediments: model/data comparison from the Eel River Margin, California." The Journal of the Acoustical Society of America **111**(6): 2621-2631.

Geissler, W. H. and W. Jokat (2004). "A geophysical study of the northern Svalbard continental margin." Geophysical Journal International **158**(1): 50-66.

Hammer, Ø., K. E. Webb and D. Depreiter (2009). "Numerical simulation of upwelling currents in pockmarks, and data from the Inner Oslofjord, Norway." Geo-Marine Letters **29**(4): 269-275.

Hernández-Molina, F. J., E. Llave and D. A. V. Stow (2008). Chapter 19 Continental Slope Contourites. Developments in Sedimentology, Elsevier. **Volume 60:** 379-407.

Ho, S., J. Cartwright and P. Imbert (2012). The formation of advancing pockmarks arrays: an interplay between hydrocarbon leakage and slope sedimentation. Abstracts, American Association of Petroleum Geologists Annual Convention and Exhibition. Long Beach, USA.

Holbrook, W. S., D. Lizarralde, I. A. Pecher, A. R. Gorman, K. L. Hackwith, M. Hornbach and D. Saffer (2002). "Escape of methane gas through sediment waves in a large methane hydrate province." Geology **30**(5): 467-470.

Holland, C. W., T. C. Weber and G. Etiope (2006). "Acoustic scattering from mud volcanoes and carbonate mounds." The Journal of the Acoustical Society of America **120**(6): 3553-3565.

Hovland, M. (1983). "Elongated depressions associated with pockmarks in the western slope of the Norwegian Trench." Marine Geology **51**(1): 35-46.

Hovland, M. (2005). "Gas Hydrates." Petroleum Geology **Gas Hydrates**: 261-268.

Hovland, M., J. V. Gardner and A. G. Judd (2002). "The significance of pockmarks to understanding fluid flow processes and geohazards." Geofluids **2**(2): 127-136.

Hovland, M. and A. G. Judd (1988). Seabed Pockmarks and Seepages. Impact on Geology, Biology and the Marine Environment. . London, Graham & Trotman Ltd.

Howe, J. A., T. M. Shimmield, R. Harland and N. Eyles (2008). "Late Quaternary contourites and glaciomarine sedimentation in the Fram Strait." Sedimentology **55**(1): 179-200.

Hustoft, S., S. Bünz, J. Mienert and S. Chand (2009). "Gas hydrate reservoir and active methane-venting province in sediments on < 20 Ma young oceanic crust in the Fram Strait, offshore NW-Svalbard." Earth and Planetary Science Letters **284**(1-2): 12-24.

Jackson, D. R., D. P. Winebrenner and A. Ishimaru (1986). "Application of the composite roughness model to high-frequency bottom backscattering." The Journal of the Acoustical Society of America **79**(5): 1410-1422.

Jessen, S. P., T. L. Rasmussen, T. Nielsen and A. Solheim (2010). "A new Late Weichselian and Holocene marine chronology for the western Svalbard slope 30,000–0 cal years BP." Quaternary Science Reviews **29**(9): 1301-1312.

Johnson, J. E., C. Goldfinger and E. Suess (2003). "Geophysical constraints on the surface distribution of authigenic carbonates across the Hydrate Ridge region, Cascadia margin." Marine Geology **202**(1–2): 79-120.

Josenhans, H. W., L. H. King and G. B. Fader (1978). "A side-scan sonar mosaic of pockmarks on the Scotian Shelf." Canadian Journal of Earth Sciences **15**(5): 831-840.

Judd, A. G. (2003). "The global importance and context of methane escape from the seabed." Geo-Marine Letters **23**(3): 147-154.

Judd, A. G. and M. Hovland (2007). Seabed fluid flow: the impact of geology, biology and the marine environment, Cambridge University Press.

Klaucke, I., W. Weinrebe, C. J. Petersen and D. Bowden (2010). "Temporal variability of gas seeps offshore New Zealand: Multi-frequency geoacoustic imaging of the Wairarapa area, Hikurangi margin." Marine Geology **272**(1): 49-58.

Kvenvolden, K. A. (1993). "Gas hydrates - geological perspective and global change." Rev. Geophys. **31**(2): 173-187.

Kvenvolden, K. A. (2000). "Gas Hydrate and Humans." Annals of the New York Academy of Sciences **912**(1): 17-22.

Laberg, J. S., M. S. Stoker, K. I. T. Dahlgren, H. d. Haas, H. Haflidason, B. O. Hjelstuen, T. Nielsen, P. M. Shannon, T. O. Vorren, T. C. E. van Weering and S. Ceramicola (2005). "Cenozoic alongslope processes and sedimentation on the NW European Atlantic margin." Marine and Petroleum Geology **22**(9-10): 1069-1088.

Landvik, J. Y., S. Bondevik, A. Elverhøi, W. Fjeldskaar, J. A. N. Mangerud, O. Salvigsen, M. J. Siegert, J.-I. Svendsen and T. O. Vorren (1998). "THE LAST GLACIAL MAXIMUM OF SVALBARD AND THE BARENTS SEA AREA: ICE SHEET EXTENT AND CONFIGURATION." Quaternary Science Reviews **17**(1-3): 43-75.

Leifer, I., J. Boles, B. Luyendyk and J. Clark (2004). "Transient discharges from marine hydrocarbon seeps: spatial and temporal variability." Environmental Geology **46**(8): 1038-1052.

Lurton, X. (2002). An introduction to underwater acoustics: principles and applications, springer.

Mangerud, J., V. Astakhov and J.-I. Svendsen (2002). "The extent of the Barents–Kara ice sheet during the Last Glacial Maximum." Quaternary Science Reviews **21**(1-3): 111-119.

Mangerud, J. A. N., T. Dokken, D. Hebbeln, B. Heggen, Ó. IngÓLfsson, J. Y. Landvik, V. Mejdahl, J. I. Svendsen and T. O. Vorren (1998). "FLUCTUATIONS OF THE SVALBARD–BARENTS SEA ICE SHEET DURING THE LAST 150 000 YEARS." Quaternary Science Reviews **17**(1-3): 11-42.

McIver, R. D. (1982). "Role of naturally occurring gas hydrates in sediment transport." AAPG Bulletin **66**(6): 789-792.

Mienert, J., M. Vanneste, S. Bünz, K. Andreassen, H. Haflidason and H. P. Sejrup (2004). "Ocean warming and gas hydrate stability on the mid-Norwegian margin at the Storegga Slide." Marine and Petroleum Geology **22**(1-2): 233-244.

Myhre, A., J. Thiede and J. Firth (1995). "1. NORTH ATLANTIC-ARCTIC GATEWAYS1."

Naudts, L., J. Greinert, Y. Artemov, S. E. Beaubien, C. Borowski and M. D. Batist (2008). "Anomalous sea-floor backscatter patterns in methane venting areas, Dnepr paleo-delta, NW Black Sea." Marine Geology **251**(3): 253-267.

Ottesen, D., J. A. Dowdeswell, J. Y. Landvik and J. Mienert (2007). "Dynamics of the Late Weichselian ice sheet on Svalbard inferred from high-resolution sea-floor morphology." Boreas: An International Journal of Quaternary Research **36**(3): 286 - 306.

Ottesen, D., J. A. Dowdeswell and L. Rise (2005). "Submarine landforms and the reconstruction of fast-flowing ice streams within a large Quaternary ice sheet: The 2500-km-long Norwegian-Svalbard margin (57-80N)." Geological Society of America Bulletin **117**(7-8): 1033-1050.

Petersen, C. and S. Buenz (2008). "High-Resolution 3D Seismic Investigation of Fluid Flow Structures in hydrated Sediments of the Vestnesa Ridge, W-Svalbard Margin."

Petersen, C. J., S. Bünz, S. Hustoft, J. Mienert and D. Klaeschen (2010). "High-resolution P-Cable 3D seismic imaging of gas chimney structures in gas hydrated sediments of an Arctic sediment drift." Marine and Petroleum Geology **27**(9): 1981-1994.

Posewang, J. and J. Mienert (1999). "High-resolution seismic studies of gas hydrates west of Svalbard." Geo-Marine Letters **19**(1-2): 150-156.

Rebesco, M. and D. Stow (2001). "Seismic expression of contourites and related deposits: a preface." Marine Geophysical Research **22**(5): 303-308.

Schauer, U., E. Fahrbach, S. Osterhus and G. Rohardt (2004). "Arctic warming through the Fram Strait: Oceanic heat transport from 3 years of measurements." J. Geophys. Res. **109**(C6): C06026.

Ślubowska-Woldengen, M., T. L. Rasmussen, N. Koç, D. Klitgaard-Kristensen, F. Nilsen and A. Solheim (2007). "Advection of Atlantic Water to the western and northern Svalbard shelf since 17,500 cal yr BP." Quaternary Science Reviews **26**(3-4): 463-478.

Smith, A. J., J. Mienert, S. Bünz and J. Greinert (2014). "Thermogenic methane injection via bubble transport into the upper Arctic Ocean from the hydrate-charged Vestnesa Ridge, Svalbard." Geochemistry, Geophysics, Geosystems.

Solheim, A., E. S. Andersen, A. Elverhøi and A. Fiedler (1996). "Late Cenozoic depositional history of the western Svalbard continental shelf, controlled by subsidence and climate." Global and Planetary Change **12**(1-4): 135-148.

Solheim, A., J. I. Faleide, E. S. Andersen, A. ElverhØI, C. F. Forsberg, K. Vanneste, G. Uenzelmann-Neben and J. E. T. Channell (1998). "LATE CENOZOIC SEISMIC STRATIGRAPHY AND GLACIAL GEOLOGICAL DEVELOPMENT OF THE EAST GREENLAND AND SVALBARD–BARENTS SEA CONTINENTAL MARGINS." Quaternary Science Reviews **17**(1-3): 155-184.

Stow, D. A. V., J.-C. Faugères, J. A. Howe, C. J. Pudsey and A. R. Viana (2002). "Bottom currents, contourites and deep-sea sediment drifts: current state-of-the-art." Geological Society, London, Memoirs **22**(1): 7-20.

Svendsen, J. I., H. Alexanderson, V. I. Astakhov, I. Demidov, J. A. Dowdeswell, S. Funder, V. Gataullin, M. Henriksen, C. Hjort, M. Houmark-Nielsen, H. W. Hubberten, Ó. Ingólfsson, M. Jakobsson, K. H. Kjær, E. Larsen, H. Lokrantz, J. P. Lunkka, A. Lyså, J. Mangerud, A. Matiouchkov, A. Murray, P. Möller, F. Niessen, O. Nikolskaya, L. Polyak, M. Saarnisto, C. Siegert, M. J. Siegert, R. F. Spielhagen and R. Stein (2004). "Late Quaternary ice sheet history of northern Eurasia." Quaternary Science Reviews **23**(11-13): 1229-1271.

Svendsen, J. I., A. Elverhmi and J. Mangerud (1996). "The retreat of the Barents Sea Ice Sheet on the western Svalbard margin." Boreas **25**(4): 244-256.

Svendsen, J. I., J. Mangerud, A. Elverhøi, A. Solheim and R. T. E. Schüttenhelm (1992). "The Late Weichselian glacial maximum on western Spitsbergen inferred from offshore sediment cores." Marine Geology **104**(1-4): 1-17.

Swift, J. H. and K. Aagaard (1981). "Seasonal transitions and water mass formation in the Iceland and Greenland seas." Deep Sea Research Part A. Oceanographic Research Papers **28**(10): 1107-1129.

Talwani, M. and O. Eldholm (1977). "Evolution of the Norwegian-Greenland Sea." Geological Society of America Bulletin **88**(7): 969-999.

Thiede, J., A. Winkler, T. Wolf-Welling, O. Eldholm, A. M. Myhre, K.-H. Baumann, R. Henrich and R. Stein (1998). "LATE CENOZOIC HISTORY OF THE POLAR NORTH ATLANTIC: RESULTS FROM OCEAN DRILLING." Quaternary Science Reviews **17**(1-3): 185-208.

Todd, B. J. (2005). "Morphology and composition of submarine barchan dunes on the Scotian Shelf, Canadian Atlantic margin." Geomorphology **67**(3): 487-500.

Vanneste, M., S. Guidard and J. Mienert (2005). "Arctic gas hydrate provinces along the western Svalbard continental margin." Norwegian Petroleum Society Special Publications **12**: 271-284.

Vanneste, M., S. Guidard and J. Mienert (2005). "Bottom-simulating reflections and geothermal gradients across the western Svalbard margin." Terra Nova **17**(6): 510-516.

Viana, A. R., W. Almeida, M. C. V. Nunes and E. M. Bulhões (2007). "The economic importance of contourites." Geological Society, London, Special Publications **276**(1): 1-23.

Vogt, P. R., K. Crane, E. Sundvor, M. D. Max and S. L. Pfirman (1994). "Methane-generated (?) pockmarks on young, thickly sedimented oceanic crust in the Arctic: Vestnesa ridge, Fram strait." Geology **22**(3): 255-258.

Vogt, P. R., J. Gardner and K. Crane (1999). "The Norwegian–Barents–Svalbard (NBS) continental margin: Introducing a natural laboratory of mass wasting, hydrates, and ascent of sediment, pore water, and methane." Geo-Marine Letters **19**(1): 2-21.

Vorren, T. O., J. S. Laberg, F. Blaume, J. A. Dowdeswell, N. H. Kenyon, J. Mienert, J. A. N. Rumohr and F. Werner (1998). "THE NORWEGIAN–GREENLAND SEA CONTINENTAL MARGINS: MORPHOLOGY AND LATE QUATERNARY SEDIMENTARY PROCESSES AND ENVIRONMENT." Quaternary Science Reviews **17**(1-3): 273-302.

Winkelmann, D., W. Geissler, J. Schneider and R. Stein (2008). "Dynamics and timing of the Hinlopen/Yermak Megaslide north of Spitsbergen, Arctic Ocean." Marine Geology **250**(1-2): 34-50.